Cell

Article

Hypothalamic neurons that mirror aggression

Graphical abstract

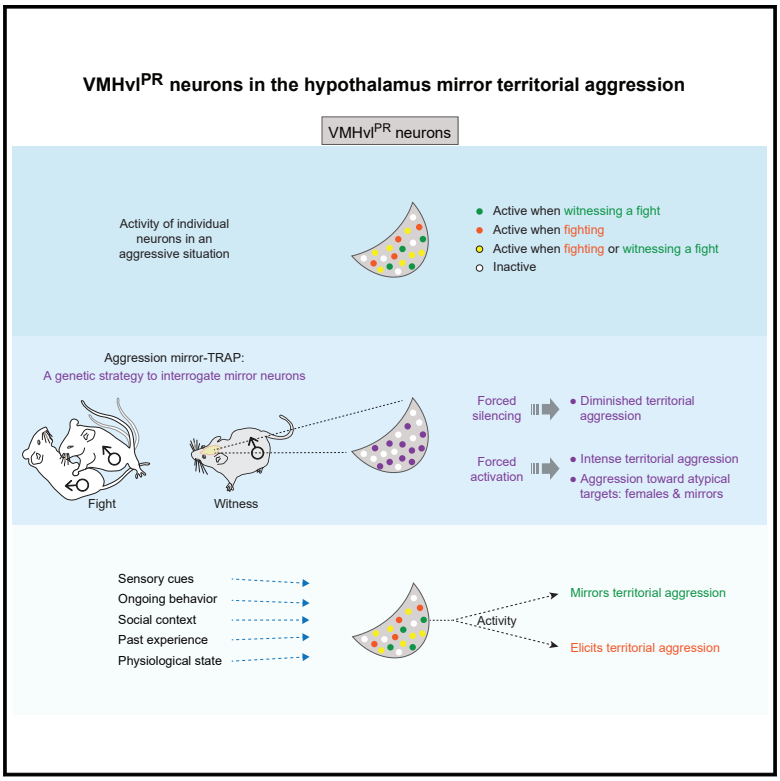

Highlights

- Individual VMHvl^{PR} neurons are co-active during both aggression or witnessing aggression
- Activity of VMHvl^{PR} neurons therefore mirrors aggression between other individuals
- Aggression-mirroring neurons are essential for territorial aggression by self
- Aggression-mirroring neurons can elicit aggression toward males, females, and mirrors

Authors

Taehong Yang, Daniel W. Bayless, Yichao Wei, ..., Liqun Luo, Shaul Druckmann, Nirao M. Shah

Correspondence

nirao@stanford.edu

In brief

Neurons whose activity mirrors fighting by other mice have been identified in the male mouse hypothalamus and shown to be functionally important for aggressive behavior.

Yang et al., 2023, Cell *186*, 1195–1211
March 16, 2023
https://doi.org/10.1016/j.cell.2023.01.022

CellPress

Cell

CellPress
OPEN ACCESS

Article

Hypothalamic neurons that mirror aggression

Taehong Yang,[1] Daniel W. Bayless,[1] Yichao Wei,[1] Dan Landayan,[1] Ivo M. Marcelo,[6,7] Yangpeng Wang,[1] Laura A. DeNardo,[4,5,8] Liqun Luo,[4,5] Shaul Druckmann,[1,2] and Nirao M. Shah[1,2,3,9,*]

[1]Department of Psychiatry and Behavioral Sciences, Stanford University, Stanford, CA 94305, USA
[2]Department of Neurobiology, Stanford University, Stanford, CA 94305, USA
[3]Department of Obstetrics and Gynecology, Stanford University, Stanford, CA 94305, USA
[4]Department of Biology, Stanford University, Stanford, CA 94305, USA
[5]Howard Hughes Medical Institute, Stanford University, Stanford, CA 94305, USA
[6]Champalimaud Neuroscience Program, Champalimaud Center for the Unknown, 1400-038 Lisbon, Portugal
[7]Department of Psychiatry, Erasmus MC University Medical Center, 3015 GD Rotterdam, the Netherlands
[8]Present address: Department of Physiology, University of California Los Angeles, Los Angeles, CA 90095, USA
[9]Lead contact
*Correspondence: nirao@stanford.edu
https://doi.org/10.1016/j.cell.2023.01.022

SUMMARY

Social interactions require awareness and understanding of the behavior of others. Mirror neurons, cells representing an action by self and others, have been proposed to be integral to the cognitive substrates that enable such awareness and understanding. Mirror neurons of the primate neocortex represent skilled motor tasks, but it is unclear if they are critical for the actions they embody, enable social behaviors, or exist in non-cortical regions. We demonstrate that the activity of individual VMHvl^{PR} neurons in the mouse hypothalamus represents aggression performed by self and others. We used a genetically encoded mirror-TRAP strategy to functionally interrogate these aggression-mirroring neurons. We find that their activity is essential for fighting and that forced activation of these cells triggers aggressive displays by mice, even toward their mirror image. Together, we have discovered a mirroring center in an evolutionarily ancient region that provides a subcortical cognitive substrate essential for a social behavior.

INTRODUCTION

Observers can acquire meaningful information from the behavior of others even when these actions are not directed to them. Such information can provide a survival advantage and, accordingly, diverse neurons are engaged in perceiving the behavior of others. Mirror neurons comprise a subset of such neurons that is active both during enactment and observation of a behavior. These cells were discovered in neocortical regions of adult primates, where they are engaged during motor skills such as reaching for an object.[1,2] There is a close correspondence between the activity of mirror neurons when the monkey is observing a behavior to which the neurons are tuned and when performing the same behavior. Given that they represent action by self and others, mirror neurons have been suggested to be important components of the cognitive substrates that enable successful social interactions. However, the functional relevance of mirror neurons in behavioral performance remains unclear. These cells are embedded within complex cortical regions, thereby rendering targeted functional interrogation a challenging proposition, especially in primates. Moreover, whether mammalian mirror neuron systems exist in evolutionarily ancient, non-cortical brain centers or are enlisted during social behaviors are open questions.

The ventromedial hypothalamus (VMH), or the nucleus of Cajal, has been studied ever since its identification in the early 20th century.[3] Experimental activation of an "attack center" located in the caudomedial hypothalamus of diverse species elicits aggression toward conspecifics, other species, and inanimate objects, even in the absence of gonadal sex hormones.[4–11] Work in mice identified the ventrolateral sector of the VMH (VMHvl) as the attack center. Targeted ablation or acute chemogenetic inhibition of VMHvl^{PR} neurons, which also co-express the estrogen receptor alpha (ERα or Esr1), reduces male territorial aggression.[9,10] Conversely, forced activation of male VMHvl^{PR}, but not neighboring, neurons, elicits aggression.[10,12] Recent work shows that VMHvl^{PR} neurons evoke aggression in a social context-sensitive manner,[10] indicating that the moniker "attack center" is simplistic and elides important properties of this neuronal population.

Given their sensitivity to social context, we wondered whether VMHvl^{PR} neurons could perceive aggressive encounters between other mice. We find that these cells are active when a mouse is fighting and also when it is observing aggression between other individuals. We employed a TRAP2-based activity-tagging approach to gain genetic access to these aggression-mirroring neurons (mirror-TRAP) and interrogate their functional relevance to aggression.[13] We find that mirror-TRAPed

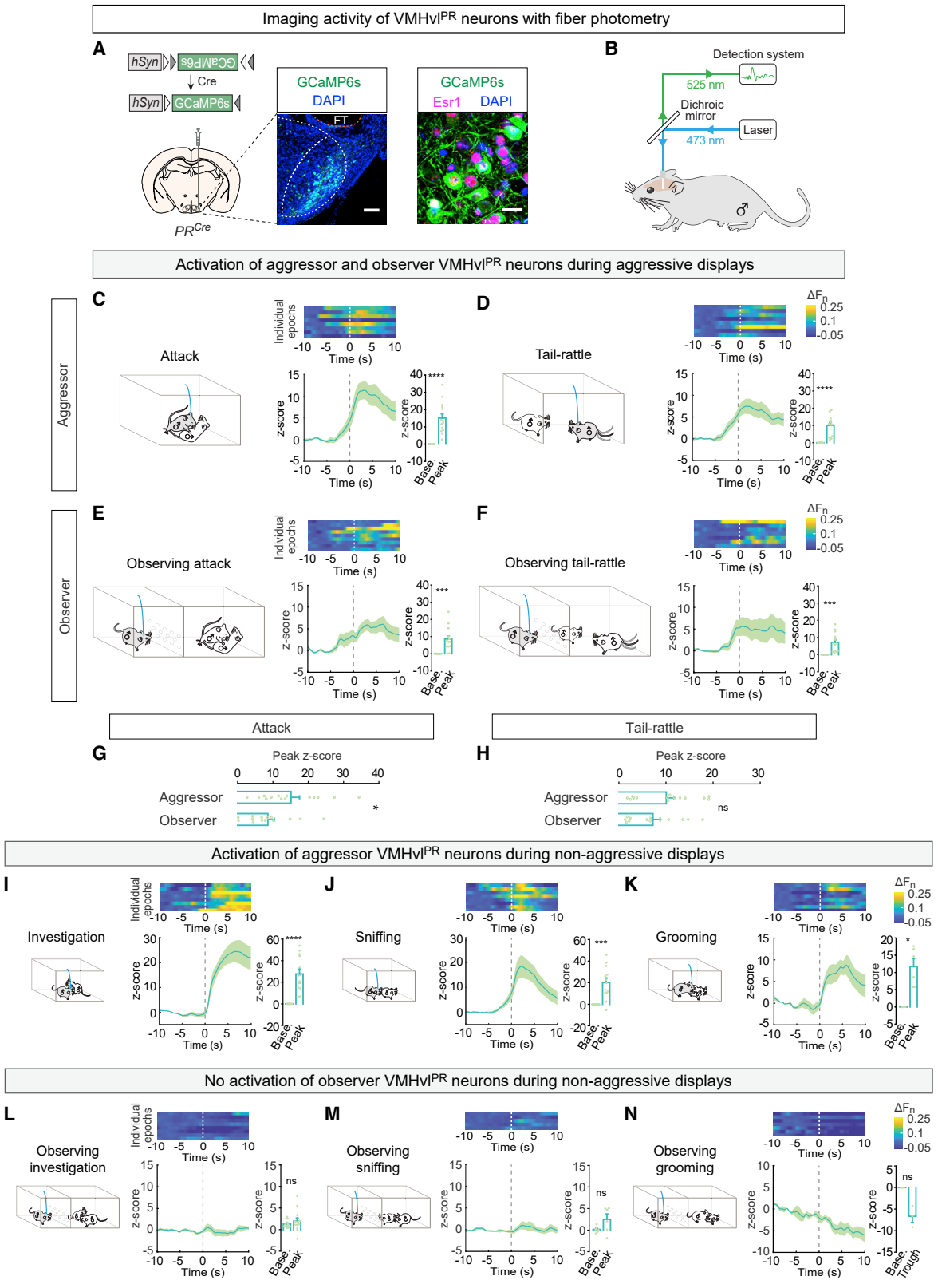

(legend on next page)

VMHvl^{PR} neurons are necessary and sufficient for fighting. Together, our findings show that VMHvl^{PR} neurons, rather than merely constituting an attack center, embody a percept of aggression that can not only trigger fighting in appropriate contexts but also monitors third-party aggressive interactions. More broadly, we have discovered a non-cortical mirror neuron system in a deeply conserved vertebrate brain region that functionally represents a social behavior essential for survival.

RESULTS

VMHvl^{PR} neurons are active during aggression by self and others

We tested whether VMHvl^{PR} neurons were responsive to aggression between other individuals. We first established the response of VMHvl^{PR} neurons in mice who were fighting so as to enable comparison with any potential responses of these cells when the mouse was witnessing aggression. We expressed GCaMP6s in VMHvl^{PR} neurons of *PR^{Cre}* mice by delivering it in a virally encoded, Cre-dependent form to the VMHvl (Figures 1A, S1A, and S1B).[9,14] We used fiber photometry to image activity of VMHvl^{PR} neurons of singly housed males following insertion of a male intruder into their cage (Figure 1B).[15,16] In this setting, the singly housed resident displayed territorial aggression toward the intruder. We observed a significant and specific increase in activity of VMHvl^{PR} cells (aggressor VMHvl^{PR} neurons) during chemoinvestigation (both anogenital and rest of the body), grooming, epochs of physical attack (such as biting or wrestling), and tail-rattling, a display that may serve as a threat signal to the opponent (Figures 1C, 1D, 1I–1K, and S1C–S1G). Our findings demonstrate activation of VMHvl^{PR} neurons during two distinct forms of aggressive displays, attacks, as described before,[17] and tail-rattling.

We devised an experimental setup in which we could image activity of VMHvl^{PR} neurons in a singly housed male who could observe, but not participate in, aggression between two males (demonstrators) (Figures 1E and 1F). Using this setup, we found that these cells (observer VMHvl^{PR} neurons) were activated when witnessing attacks and tail-rattles (Figures 1E, 1F, and S1H). The increase in activity was larger in aggressor than observer VMHvl^{PR} neurons for attacks but comparable for tail-rattling (Figures 1G and 1H). In contrast to the activity of VMHvl^{PR} aggressor neurons, observer neurons were activated during aggressive displays but not during other social interactions such as chemoinvestigation or grooming (Figures 1I–1N). Our findings show that VMHvl^{PR} neurons are active when a mouse is fighting and when it witnesses fighting between others.

We wondered whether other centers essential for aggression also exhibit aggression-mirroring. The male bed nucleus of the stria terminalis (BNST) recognizes sex of conspecifics and is required for territorial aggression.[18,19] We recently identified tachykinin 1-expressing BNST (BNST^{Tac1}) neurons as the transcriptomically defined BNST population in males that regulates sex recognition and aggression.[20] Accordingly, we sought to test whether BNST^{Tac1} neurons mirror aggression by expressing GCaMP6s in these cells of Tac1^{Cre} males (Figures S1I–S1K and S1M). BNST^{Tac1} neurons were activated both when residents first encountered an intruder in their cage and when they attacked the intruder (Figures S1J–S1K). However, BNST^{Tac1} neurons were not discernibly activated when witnessing aggression (Figure S1L). Together, our findings show that VMHvl^{PR} neurons exhibit mirroring properties for aggression and that such mirroring is not a feature of all populations that regulate aggression.

Visual input, but not social experience, is essential for mirroring by VMHvl^{PR} neurons

Sensory input and experience powerfully modulate male mouse territorial aggression.[10,21–23] We first sought to understand the nature of sensory cues that elicit aggression-mirroring. Observer VMHvl^{PR} neurons are not activated during non-aggressive displays, suggesting that they would not be activated by locomotor activity of a demonstrator. Indeed, they did not discernibly respond to running-wheel use by self or demonstrator (Figures S1N–S1P); importantly, these neurons were active during enactment or observation of aggression (Figures 1C–1F), indicating that the lack of response with a running-wheel reflected specificity for fighting rather than failure of functional GCaMP6s expression.

We wondered whether activation of observer VMHvl^{PR} neurons during aggressive displays obscured subtler activation during non-aggressive displays such as sniffing. Males null for Trpc2, a cation channel essential for pheromone sensing by

Figure 1. VMHvl^{PR} neurons exhibit aggression-mirroring

(A) Strategy to express GCaMP6s in VMHvl^{PR} neurons. GCaMP6s expression in VMHvl^{PR} neurons shown in coronal section (middle), with dashed white lines outlining VMH and, more laterally on the right, VMHvl, and dashed orange line outlining the fiber optic tract (FT) dorsally. GCaMP6s+ cells express Esr1 (right).

(B) Schematic of fiber photometry setup in freely moving mice.

(C and D) Aggressor VMHvl^{PR} neurons are activated during attack (C) and tail-rattling (D). Dashed vertical line in the peri-event time plot (PETP) shows onset of behavioral display in all figures. Heatmap above PETPs here and other figures, unless otherwise specified, shows normalized fluorescence signal from a single representative experimental male during individual sequential epochs of that particular behavior. F_n represents fractional change in fluorescence from baseline fluorescence preceding the event. Experimental male is shaded gray in schematic panels of all figures.

(E and F) Observer VMHvl^{PR} neurons show mirroring activity when witnessing attacks (E) or tail-rattles (F) by demonstrator males.

(G) Aggressor VMHvl^{PR} neurons show higher peak activation during attacks than observer VMHvl^{PR} neurons.

(H) No difference in peak activation between aggressor and observer VMHvl^{PR} neurons during tail-rattling.

(I–K) Aggressor VMHvl^{PR} neurons are activated during investigation (chemoinvestigation of non-anogenital regions) (I), sniffing (anogenital chemoinvestigation) (J), and grooming (K).

(L–N) No discernible activation of observer VMHvl^{PR} neurons during investigation (L), sniffing (M), and grooming (N).

Mean (dark trace) ± SEM (lighter shading) of *Z*-scored activity shown in PETPs of all figures. Mean ± SEM, bar graphs.

Base., baseline fluorescence signal; Peak, peak amplitude of fluorescence signal.

Scale bars, 100 μm (A, middle) and 20 μm (A, right). n = 14 *PR^{Cre}* males. ns = not significant, *p < 0.05, ***p < 0.001, ****p < 0.0001.

See also Figure S1.

vomeronasal organ (VNO) neurons in the nose, are not aggressive but show non-aggressive behaviors such as sniffing.[24,25] We used fiber photometry to image VMHvl^{PR} neurons of *PR^{Cre}* males observing interactions between *Trpc2*$^{-/-}$ demonstrators. Observer VMHvl^{PR} cells were not discernibly activated in this paradigm (Figures S1Q–S1R), further underscoring the specificity of the response of these neurons to attacks and tail-rattles.

We tested whether activation of observer VMHvl^{PR} neurons reflected observers mimicking aggressive displays of demonstrators, in effect with shadow boxing-type movements. However, observers generated very few tail-rattles (<2/assay) or rapid movements ($\leq$1/assay) that could be construed as chasing during aggression in comparison to the demonstrators (Figures S2A and S2B). Observers generated comparably few tail-rattles or rapid movements when they were observing demonstrators fight or *Trpc2*$^{-/-}$ demonstrators engage in non-aggressive interactions (Figures S2A and S2B). The few tail-rattles or rapid movements of observers also did not correlate with the increased activity of their VMHvl^{PR} neurons, which coincided with aggressive displays by demonstrators (data not shown). Thus, observers do not appear to engage in overt aggressive displays themselves when witnessing those by others.

The observer paradigm we had designed allowed mice to access at least visual and chemosensory cues emanating from demonstrators through a transparent, perforated partition. Male pheromones detected by chemosensory neurons in the VNO and main olfactory epithelium (MOE) are essential for triggering aggression from other males.[24–27] We imaged VMHvl^{PR} neurons of *Trpc2*$^{-/-}$ males while they were observing demonstrators fight (Figure 2A). Similar to *Trpc2*$^{+/+}$ observer VMHvl^{PR} neurons, *Trpc2*$^{-/-}$ observer VMHvl^{PR} cells responded to bouts of attacks and tail-rattling (Figures 2B and 2C). The peak amplitude of this activity appeared comparable to that seen in wild-type (WT) VMHvl^{PR} observer neurons (Physical attack: WT 8.6 ± 1.8 and *Trpc2*$^{-/-}$ 4.8 ± 1.6, n $\geq$ 9, p = 0.14; Tail-rattle: WT 7.2 ± 1.5 and *Trpc2*$^{-/-}$ 5.1 ± 1.7, n $\geq$ 9, p = 0.38; *Z*-scored ΔF/F, mean ± SEM). *Trpc2*$^{-/-}$ males are not aggressive, but their VMHvl^{PR} neurons responded to chemoinvestigation of male intruders similar to *Trpc2*$^{+/+}$ aggressor VMHvl^{PR} cells (Figures 1I, 1J, and S2C–S2E). The response of *Trpc2*$^{-/-}$ VMHvl^{PR} neurons during chemoinvestigation was smaller than their WT counterparts, in accord with an important role for Trpc2 in pheromone signal transduction. The perforated partition of the testing area enables observers access to volatile cues, which can be sensed by both VNO and MOE neurons. Males genetically disabled for MOE signaling are smaller than WT siblings, making it challenging to perform Ca^{++} imaging. As an alternative, we replaced the perforated partition with a solid, transparent partition and mounted a solid, transparent ceiling over the demonstrators. We reasoned that this setup would likely minimize access of demonstrator pheromones to the observers. Nevertheless, we observed activation of observer VMHvl^{PR} neurons at levels that appeared similar to those across a perforated partition (Physical attack: perforated 8.6 ± 1.8 and solid 6.2 ± 0.6, n $\geq$ 6, p = 0.35; Tail-rattle: perforated 7.2 ± 1.5 and solid 3.8 ± 1.4, n $\geq$ 6, p = 0.21; *Z*-scored ΔF/F, mean ± SEM) (Figures S2F–S2I). Although we cannot exclude the possibility that observers could access pheromonal cues in this setup, our findings indicate that pheromone sensing may not be essential for aggression-mirroring by VMHvl^{PR} neurons.

The testing arena we had designed was illuminated and we wondered whether visual input was required for aggression-mirroring. Accordingly, we used an arena with a perforated partition and illuminated it in the infrared spectrum (850 nm, $\leq$1 lux) to which mice are insensitive (Figure 2D). In this setting, observer VMHvl^{PR} neurons showed no discernible activation to physical attacks or tail-rattles. (Figures 2E and 2F). The absence of activation of observer neurons under infrared illumination does not reflect lack of functional GCaMP6s expression because these cells were activated when the males were used as aggressors (Figures S2J–S2L). We reasoned that if visual cues play a critical role in aggression-mirroring then VMHvl^{PR} neurons would not be activated when the observer faced away from demonstrators. Indeed, we found that, even under regular lighting, observer VMHvl^{PR} neurons were not activated when the male was facing away from demonstrators engaged in aggression (Figures S2M−S2N). Together, our findings demonstrate a critical role for visual input in aggression-mirroring by VMHvl^{PR} neurons.

Previous studies have identified mirror neurons in the context of learned motor displays, leading to the notion that these cells may have evolved to acquire skilled behaviors.[28] Here, we have identified mirror neurons for male territorial aggression in mice, an innate behavior that can be displayed without prior experience. We cannot exclude the possibility that aggression-mirroring by VMHvl^{PR} neurons emerges following social experience because observers had previously mated and fought. Accordingly, we imaged GCaMP6s-expressing VMHvl^{PR} neurons in observers who were socially naive for sexual behavior and territorial aggression. Socially naive observer VMHvl^{PR} neurons responded to aggressive displays between demonstrators as well as in subsequent assays when these males were first used as aggressors (Figures 2G–2I and S2O–S2Q). The response of naive observer neurons was similar to that of observer neurons in socially experienced males (Attack: naive, 6.5 ± 0.9 and experienced, 8.6 ± 1.8, p = 0.41; Tail-rattle: naive, 9.3 ± 2 and experienced, 7.2 ± 1.5, p = 0.42; n $\geq$ 8; *Z*-scored ΔF/F mean ± SEM). The mirroring response of VMHvl^{PR} neurons in experienced males preceded the actual onset of fighting, whereas that in naive males appeared at the onset of aggression (Figures 1E, 1F, and 2H–2I), suggesting that fighting experience modulates the mirroring activity of these cells. Nevertheless, VMHvl^{PR} neurons exhibit aggression-mirroring in males not previously tested in aggression assays. Together, our findings show that visual input, but not prior experience, is critical for aggression-mirroring by VMHvl^{PR} cells.

Individual VMHvl^{PR} neurons are co-activated when males fight or observe aggression

We next determined whether individual VMHvl^{PR} neurons were active during enactment and observation of aggressive displays. Fiber photometry provides a readout of ensemble activity and cannot distinguish whether the same, distinct, or overlapping subsets of cells are activated in aggressors and observers (Figure 3A). We performed miniscope imaging to follow individual GCaMP6s-labeled VMHvl^{PR} neurons of singly housed males

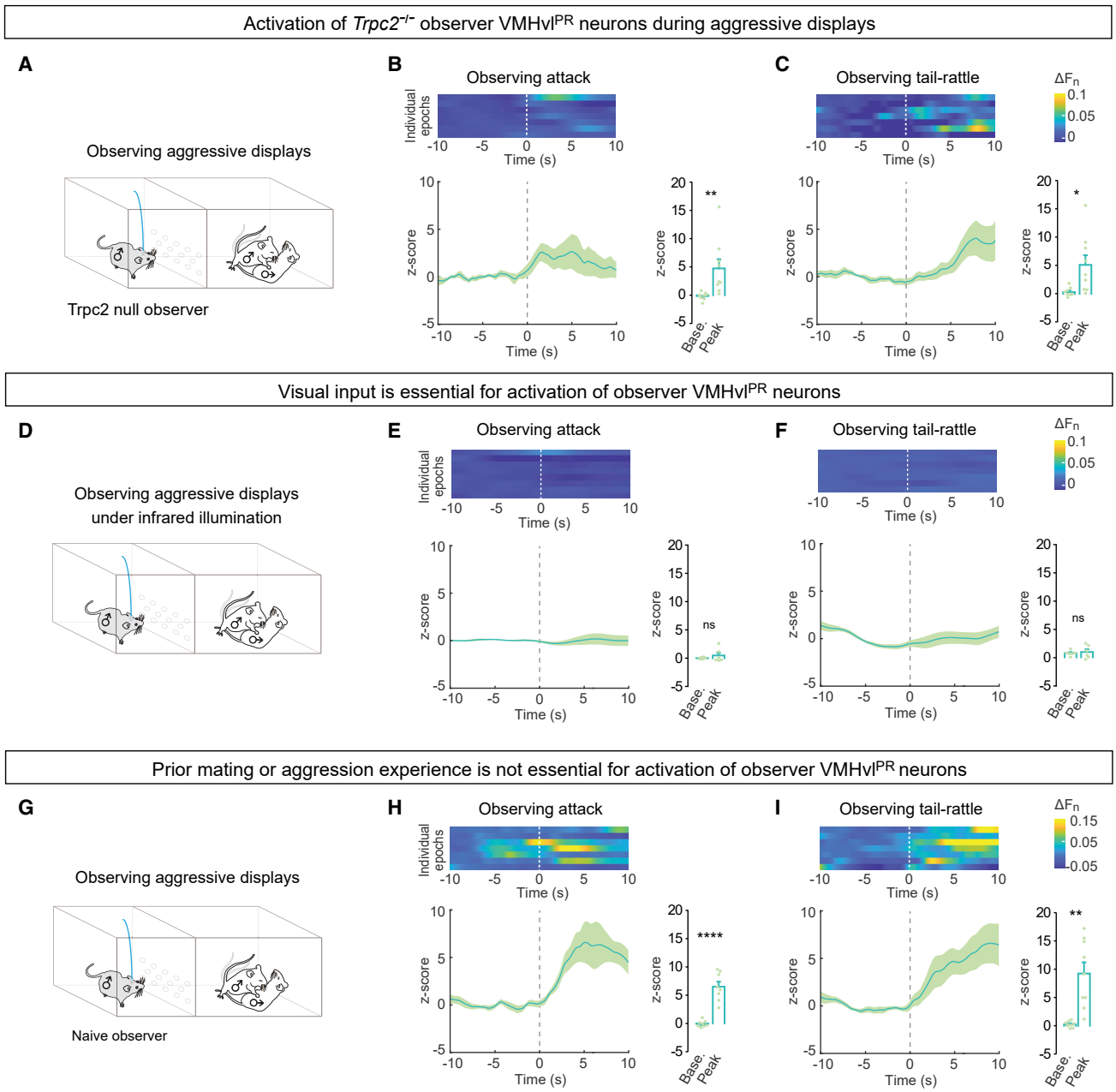

Figure 2. Aggression-mirroring by VMHvl^{PR} neurons requires visual input

(A–C) Imaging observer VMHvl^{PR} neurons of Trpc2 null males witnessing aggression.(A) Schematic of behavioral paradigm.

(B and C) Activation of observer VMHvl^{PR} neurons during attacks (B) and tail-rattling (C).

(D–F) Imaging observer VMHvl^{PR} neurons witnessing aggression under infrared illumination.

(D) Schematic of behavioral paradigm.

(E and F) No discernible activation of observer VMHvl^{PR} neurons during attacks (E) or tail-rattling (F).

(G–I) Imaging observer VMHvl^{PR} neurons of socially naive males witnessing aggression.

(G) Schematic of behavioral paradigm.

(H and I) Activation of observer VMHvl^{PR} neurons during attacks (H) and tail-rattling (I).

Mean ± SEM n = 9 $PR^{Cre};Trpc2^{-/-}$ (B) and (C), 6 PR^{Cre} (E) and (F), 7 PR^{Cre} (H) and (I) males. *p < 0.05, **p < 0.01, ****p < 0.0001.

See also Figure S2.

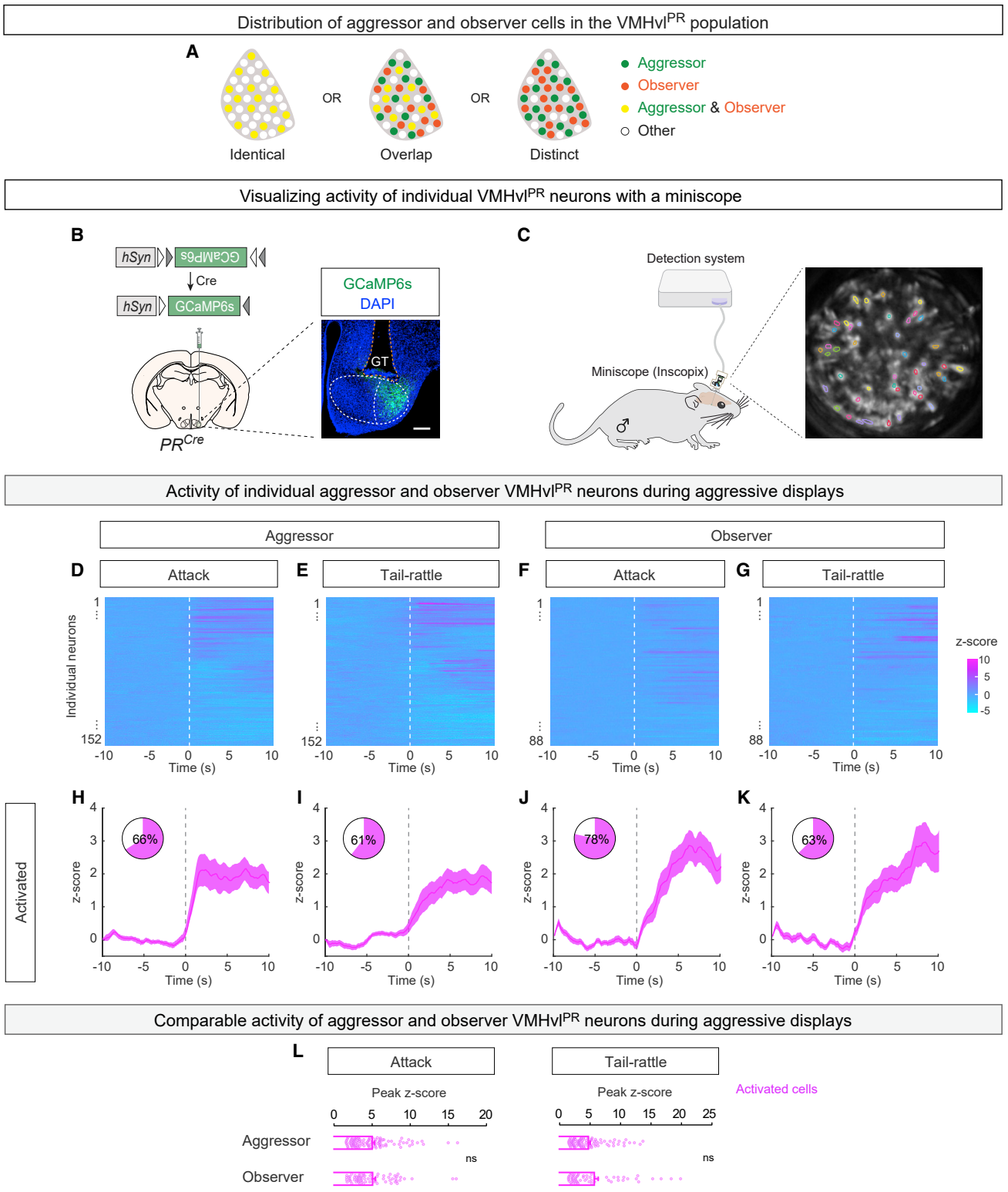

Figure 3. Individual aggressor and observer VMHvl^{PR} neurons are activated during attacks and tail-rattles

(A) There could be complete, partial, or no overlap between aggressor and observer VMHvl^{PR} neurons.

(B) Strategy to express GCaMP6s in VMHvl^{PR} neurons (left). Coronal section through the VMH with GRIN lens track (GT) visible dorsal to the GCaMP6s+ cells in the VMHvl (right). Dashed white lines outline VMH and VMHvl and dashed orange lines outline the GT.

(legend continued on next page)

deployed as aggressors and observers in separate assays (Figures 3B–3L).[29–31] Using stringent noise reduction and segmentation pipelines,[32] we identified 152 and 88 neurons with reliable GCaMP6s fluorescence in aggressors and observers, respectively (n = 5 males).

We first characterized these cells separately in aggressors and observers. We found that most (61%–78%) VMHvl^{PR} neurons were activated in aggressors and observers during attacks and tail-rattling (Figures 3D–3K and S3A–S3D). Peak activation of individual neurons was comparable during performance or observation of attacks or tail-rattles (Figure 3L). A small subset of neurons (16%–34%) was inhibited during attacks or tail-rattles in aggressors and observers, and a minority of cells (5%–11%) showed no discernible changes in fluorescence (Figures S3A–S3M), consistent with prior work showing that some VMHvl neurons were inhibited or quiescent in aggressors.[7,17] As with activated neurons, the maximal inhibition of individual VMHvl^{PR} neurons was similar between participants and witnesses (Figure S3M). To test whether individual neurons alternated between being activated and inhibited during different epochs of attacks or tail-rattling, we shuffled the GCaMP6s signal of individual cells for the entire period of behavioral testing. A comparison of shuffled and unmanipulated datasets showed that individual VMHvl^{PR} neurons in both aggressors and observers were reliably either activated or inhibited (Figure S3N).

Although fiber photometry showed increased activation during attack compared to observing attack, this difference was not apparent with miniscope imaging. This likely reflects the fact that fiber photometry captures fluorescence changes from multiple cellular compartments whereas our miniscope analysis pipeline reveals activity restricted to the soma.[33] Miniscope imaging revealed VMHvl^{PR} neurons that were inhibited during attacks, a feature that could not have been predicted from fiber photometry but is consistent with prior studies of VMHvl neurons during aggression.[7,17] Averaging the response of all aggressor or observer VMHvl^{PR} neurons showed a net activation of these cells during attack or tail-rattle, consistent with findings from fiber photometry (Figures S3I–S3M). Together, we can reliably image activity of individual VMHvl^{PR} neurons in aggressors and observers.

We determined whether individual neurons were co-activated in aggressors and observers during an aggressive display. Accordingly, we identified 69 VMHvl^{PR} neurons that were reliably visualized during both aggressor and observer sessions (Figure S4A). In principle, identical, overlapping, or completely distinct sets of these VMHvl^{PR} neurons could be activated in aggressors and observers (Figure 3A). We found that overlapping sets of VMHvl^{PR} neurons were activated during performance or observation of physical attacks (Figures 4A–4D, S4B, and Table S1). Peak activation of the population was higher when observing rather than performing physical attacks, a difference that could reflect higher net activation during observation or differences in activation dynamics between these two paradigms. The peak as well as net activation of individual VMHvl^{PR} cells were comparable between participants and witnesses during physical attacks, suggesting that this shared neuronal population exhibited different dynamics between mirroring and performing attacks. Overlapping sets of VMHvl^{PR} neurons were also activated when the mouse was performing or observing tail-rattles, with activation dynamics and peak as well as net activation of individual cells being comparable in participants and witnesses (Figures 4E–4H and S4B). Our findings show that individual VMHvl^{PR} neurons are co-activated during performance and observation of attacks or tail-rattles.

In primates, at least two classes of mirror neurons have been described, those whose activity represents identical movements (strictly congruent) or movements directed toward the same goal (broadly congruent) during observation and performance of a behavior.[34] We wished to determine whether aggression-mirroring VMHvl^{PR} neurons were narrowly or broadly tuned to attacks and tail-rattles. We first tested whether activity of individual neurons could even represent both attacks and tail-rattles in aggressors or observers. We found that single aggressor or observer VMHvl^{PR} neurons were activated during both physical attacks and tail-rattles, with comparable dynamics, peak activation of individual cells, and net activation (Figures S4C–S4J). Thus, attacks and tail-rattles, routines with distinct motor actions, were reflected in activation of individual VMHvl^{PR} neurons of aggressors or observers. We next tested whether single neurons could represent attacks and observing tail-rattles or vice versa. Overlapping sets of VMHvl^{PR} cells were activated during performance and observation of attacks and tail-rattles, respectively, and vice versa (Figures 4I–4P and Table S1). Although activation dynamics differed subtly between participants and witnesses, the peak and net activation of individual VMHvl^{PR} neurons were similar in both comparisons. Together, our findings demonstrate that individual VMHvl^{PR} neurons can represent distinct aggressive motor actions, and, in this sense, they show broadly congruent mirroring properties.

Finally, we tested whether there were VMHvl^{PR} neurons whose activity during attacks or tail-rattles was restricted to aggressors or observers. We found 2 VMHvl^{PR} neurons whose activity reflected performance but was unchanged during observation of attacks or tail-rattles. In other words, ~3% (2/69) of VMHvl^{PR}

(C) Setup for miniscope imaging of VMHvl^{PR} neurons in freely moving mice. Inset shows raw GCaMP6s fluorescence overlaid with contours of segmented cells that were significantly active during behavioral testing.
(D–G) Individual aggressor or observer VMHvl^{PR} neurons are activated, inhibited, or silent during attacks (D) and (F) or tail-rattles (E) and (G). Raster of mean activity of individual neurons from 5 males shown as heatmap. Cells are ordered starting with most activated on top and most inhibited at the bottom, and row numbers do not correspond to the same cells across panels. Peaks and troughs of GCaMP6s fluorescence of neurons classified as activated or inhibited corresponded to Z scores >1.5 and <−1.5, respectively, in these and subsequent panels of Figures 3, S3, 4, and S4.
(H–K) Population dynamics of activated aggressor and observer VMHvl^{PR} neurons, with inset pie-charts showing percent of activated cells for attacks (H) and (J) and tail-rattles (I) and (K).
(L) No difference in peak amplitude of activity of activated VMHvl^{PR} neurons between aggressors and observers for either attacks or tail-rattles.
Mean ± SEM n = 152 aggressor and 88 observer VMHvl^{PR} neurons from 5 PR^{Cre} males. Scale bar, 200 μm.
See also Figure S3.

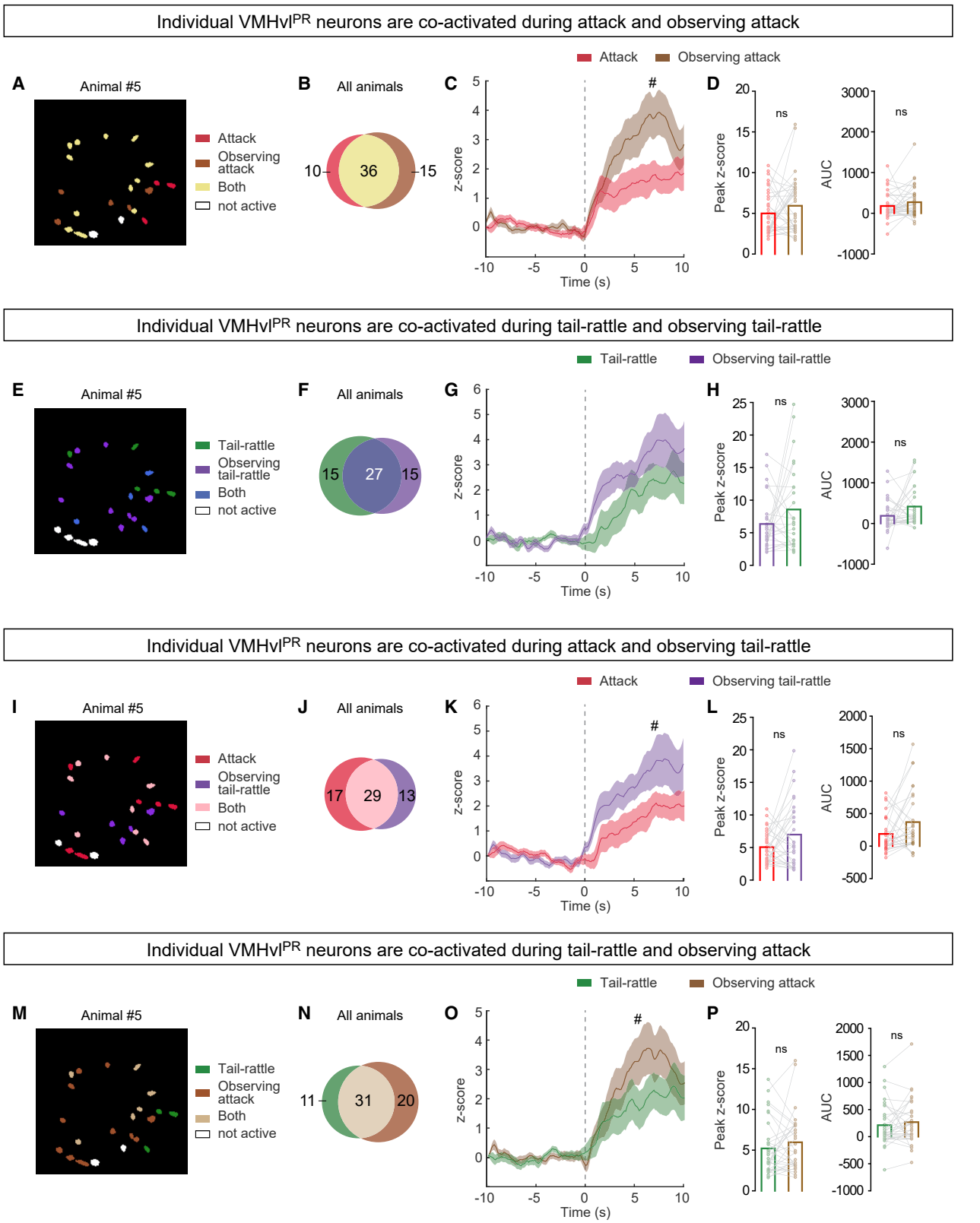

(legend on next page)

neurons appeared to be "pure" action neurons. However, we did not find cells whose activity changed exclusively during observation of aggressive displays. In summary, we find that overlapping sets of VMHvl^{PR} neurons are activated during performance and observation of attacks and tail-rattles.

An aggression mirror-TRAP strategy to capture observer VMHvl^{PR} neurons

We wished to test the functional relevance of observer VMHvl^{PR} neurons in territorial aggression. Given the heterogeneity of the VMHvl,[20,35,36] we first needed to establish a genetic means to specifically interrogate observer cells. Accordingly, we tested whether TRAP2 would enable genetic access to this population. In TRAP2, a neuronal population that expresses Fos—a surrogate for neuronal activation—co-expresses Cre^{ERT2}, and Cre^{ERT2} switches on expression of Cre-dependent transgenes following provision of the ligand 4-hydroxytamoxifen (4OHT)[13,37] (Figure 5A). Aggression induces Fos in VMHvl^{PR} neurons, and we tagged aggression-activated VMHvl neurons of *TRAP2;Ai14* males with tdTomato[7,38] (Figure 5B, left). We allowed these males to view demonstrators fighting and immunolabeled observation-activated neurons for Fos (Figure 5B, right). In accord with our miniscope results, we found that most aggression-TRAPed (tdTomato+) VMHvl neurons expressed Fos upon observing aggression (Figure 5C). The fact that not all tdTomato+ cells were Fos+ is in agreement with prior work showing that TRAP2 captures a subset of Fos+ neurons.[13,37] Indeed, an indistinguishable percent of tdTomato+ neurons was Fos+ following observation of aggression or performing another round of aggression (Figures 5B and 5C). By contrast, far fewer neurons tagged with tdTomato in their home cage without social interactions expressed Fos induced by observing aggression (Figure S5A). Together, these results further validate our miniscope findings and provide a genetic strategy to interrogate observer neurons.

We employed an aggression mirror-TRAP strategy to express GCaMP6s in observer VMHvl neurons and tested whether this would yield sufficient GCaMP6s+ cells for fiber photometry during performance or observation of aggression (Figure 5D). We found that mirror-TRAPed cells were activated when males attacked or tail-rattled toward an intruder male (Figures S5B and S5C). These GCaMP6s+ VMHvl neurons were also specifically activated when males observed aggressive displays between demonstrators (Figures 5E, 5F, S5D, and S5E). These findings indicate a close correspondence between TRAP2-tagged VMHvl and VMHvl^{PR} mirror neurons. Within the VMH, only VMHvl^{PR} neurons, which also co-express Esr1, appear to be critical for territorial aggression.[9,10,12,20] The aggression-mirror TRAP strategy is not contingent on PR expression, leaving open the possibility that we were genetically tagging a different VMHvl population. To exclude this, we co-labeled tdTomato+, mirror-TRAPed observer VMHvl neurons with Esr1. We found that most tdTomato+ VMHvl neurons are Esr1+ (Figure S5F). Together, our findings show that our aggression mirror-TRAP strategy can be used to express transgenes of choice in VMHvl^{PR} mirror neurons.

Aggression-mirroring VMHvl neurons are essential for male territorial aggression

The overlap of neurons active when witnessing and performing aggression suggested the possibility that these cells were functionally relevant for fighting. We tested this hypothesis, using aggression mirror-TRAP to inhibit aggression-mirroring neurons. We delivered a virally encoded, Cre-dependent inhibitory chemogenetic actuator,[39] DREADDi, to the VMHvl and captured neurons activated in observer TRAP2 males using 4OHT (Figures 6A and S6B). We tested these males as residents following administration of Clozapine-N-oxide (CNO) or vehicle in a resident-intruder territorial aggression assay (Figure 6B). Animals given CNO showed a ~3-fold reduction in the likelihood of initiating attacks or tail-rattles (Figures 6C and 6D). Furthermore, they fought less intensely, with a >10-fold reduction in time spent attacking the intruder (Figures 6E–6G). CNO administration did not reduce sniffing or other non-aggressive social interactions (Figure S6A and data not shown), indicating that the diminution in aggression did not reflect a pervasive attenuation of social interactions. Targeted ablation or acute inhibition of VMHvl^{PR} neurons leads to a subtle reduction in male sexual behavior.[9,10] We tested whether inhibiting aggression mirror-TRAPed VMHvl neurons would also suppress mating (Figure S6C). CNO-administered residents performed comparably to control residents in mating with female intruders, both in the likelihood to initiate mating routines and patterning of sexual behavior (Figures S6D–S6H). In summary, aggression-mirroring VMHvl neurons play a specific and essential role in the display of male territorial aggression.

To test the specificity of our aggression mirror-TRAP strategy, we delivered the Cre-dependent DREADDi to the VMHvl and

Figure 4. Individual VMHvl^{PR} neurons are co-activated during aggressor and observer paradigms

(A–D) Co-activation of individual neurons during attacks in aggressor and observer paradigms. Segmented cells during representative imaging sessions of a male tested as aggressor or observer (A). Overlapping sets of VMHvl^{PR} neurons are co-activated in participants and witnesses (B), with distinct activation dynamics at a few time points (C), but comparable peak amplitude of, or net, activation (D).

(E–H) Co-activation of individual neurons during tail-rattles in aggressor and observer paradigms. Segmented cells during representative imaging sessions of a male tested as aggressor or observer (E). Overlapping sets of VMHvl^{PR} neurons are co-activated in participants and witnesses during tail-rattles (F), with comparable activation dynamics (G) and peak amplitude of, or net, activation (H).

(I–L) Co-activation of individual neurons during attacks and observation of tail-rattles. Segmented cells during representative imaging sessions of a male tested as aggressor or observer (I). Overlapping sets of VMHvl^{PR} neurons are co-activated in participants and witnesses (J), with distinct activation dynamics at a few time points (K), but comparable peak amplitude of, or net, activation (L).

(M–P) Co-activation of individual neurons during tail-rattles and observation of attacks. Segmented cells during representative imaging sessions of a male tested as aggressor or observer (M). Overlapping sets of VMHvl^{PR} neurons are co-activated in participants and witnesses (N), with distinct activation dynamics at a few time points (O), but comparable peak amplitude of, or net, activation (P).

Mean ± SEM AUC, area under the curve. n = 5 PR^{Cre} males. #, significant difference at multiple time points.

See also Figure S4 and Table S1.

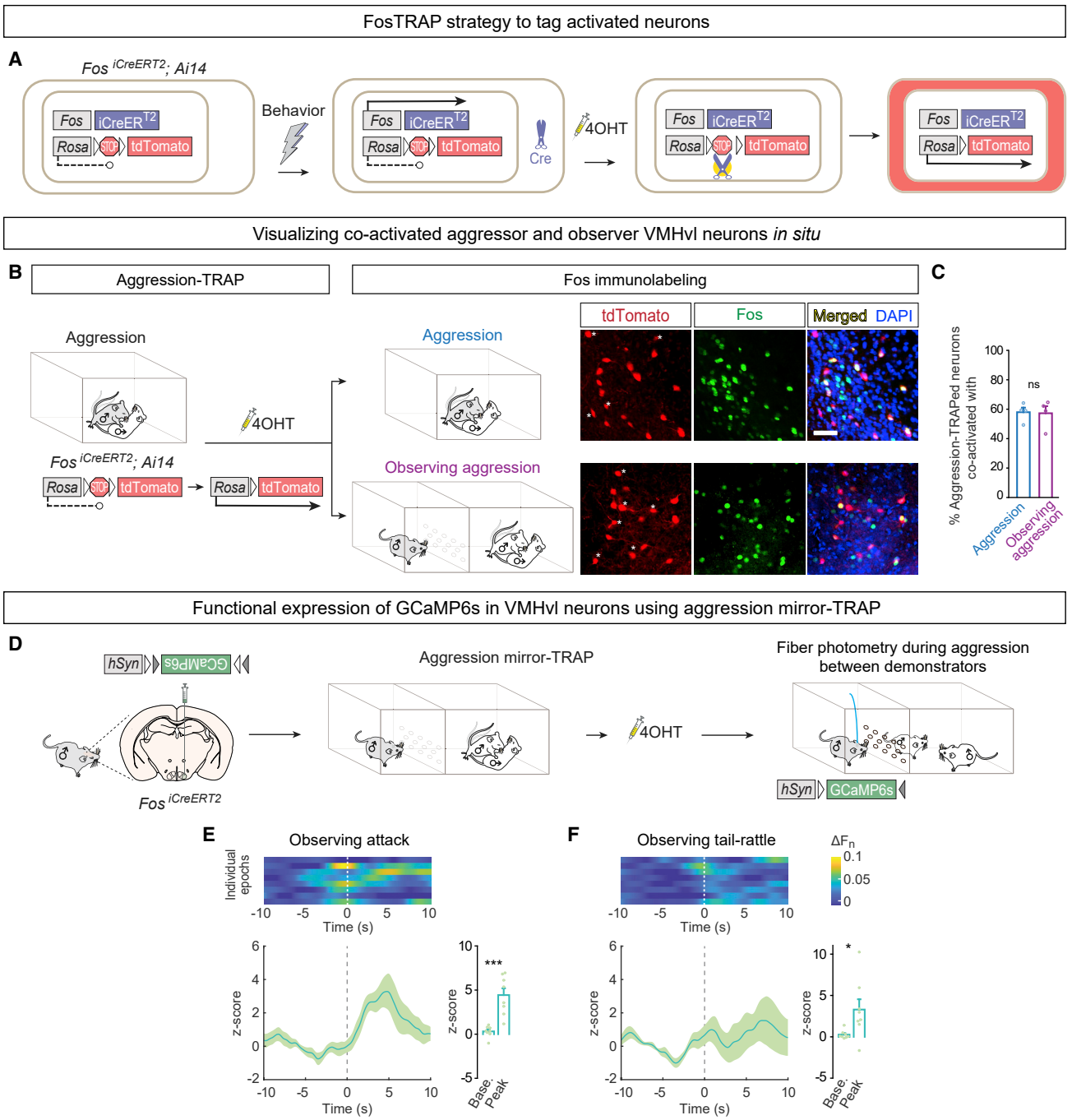

Figure 5. An aggression mirror-TRAP strategy indelibly tags observer VMHvl neurons

(A) Schematic of FosTRAP2 strategy to genetically tag activated, Fos-expressing neurons.

(B and C) Aggression-activated, FosTRAP2-tagged neurons (Aggression-TRAP, tdTomato+, red) show comparable Fos induction (green) following performance or observation of aggression. Asterisks (B) label tdTomato+ and Fos− cells. For all TRAPing studies in this and subsequent figures, mice were subjected to two rounds of the behavior being tested and provision of 4OHT to maximize number of neurons expressing the Cre-dependent transgene.

(D) Schematic of aggression mirror-TRAP strategy to express GCaMP6s in VMHvl neurons for fiber photometry.

(E and F) Significant activation of aggression mirror-TRAPed, GCaMP6s+ VMHvl neurons when the male is observing attacks (E) or tail-rattles (F).

Mean ± SEM n = 4 (B) and (C) *Fos*^{iCreERT2};*Ai14* and 8 (E) and (F) *Fos*^{iCreERT2} males. *p < 0.05, ***p < 0.001. Scale bar, 50 μm.

See also Figure S5.

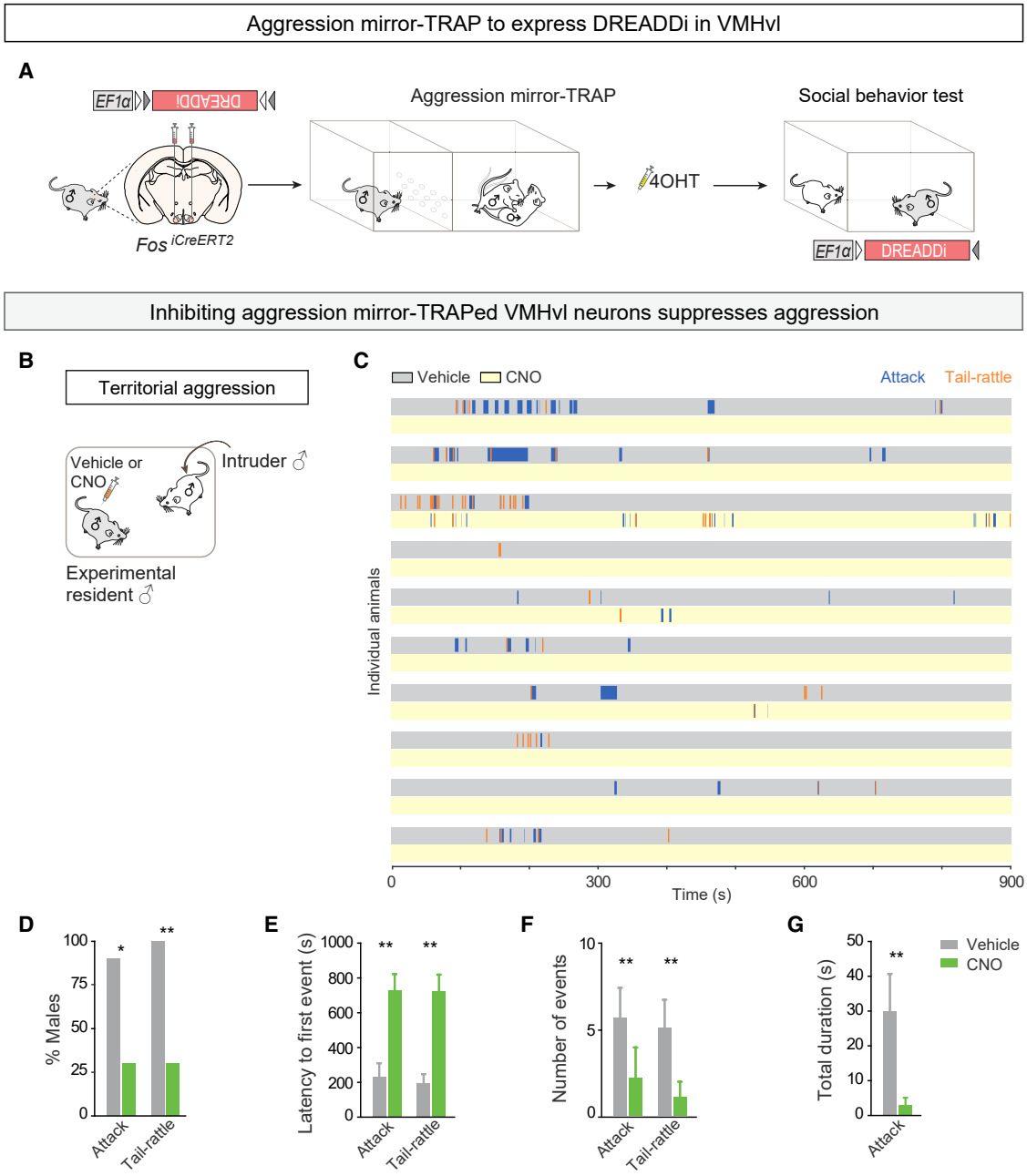

Figure 6. Activity of aggression-mirroring VMHvl neurons is essential for territorial aggression

(A) Schematic of aggression mirror-TRAP strategy to express the inhibitory chemogenetic actuator DREADDi in VMHvl neurons.

(B) Schematic of resident-intruder test of territorial aggression, with the aggression mirror-TRAPed resident male expressing DREADDi in VMHvl cells.

(C) Rasters of individual resident males showing reduced aggression upon inhibition of aggression-mirroring VMHvl neurons. In this and subsequent figures, each consecutive pair of vehicle and CNO rasters, starting from the top row, represents behavioral displays of a resident encountering an unfamiliar intruder on different days in his cage. Rasters in this and subsequent figures are only shown for males displaying behaviors being tested in at least one condition (vehicle or CNO).

(D–G) Inhibition of aggression-mirroring VMHvl neurons reduces the likelihood that males attack or tail-rattle (D), increases the latency to initiate either of these two behaviors (E), and reduces the number and duration of aggressive events (F) and (G).

Mean ± SEM n = 10 *Fos*^{iCreERT2} males. *p < 0.05, **p < 0.01.

See also Figure S6.

TRAPed neurons in observers viewing non-aggressive social interactions between *Trpc2*$^{-/-}$ demonstrators (Figures S6I–S6J). We tested these observers as residents in assays of territorial aggression and mating. We found that CNO had no discernible effect on aggression and mating routines with males and females, respectively (Figures S6K–S6T). We conclude that our aggression mirror-TRAP strategy effectively captures aggression-mirroring VMHvl^{PR} neurons and that these cells are essential for the WT display of territorial fighting.

Aggression-mirroring VMHvl neurons are sufficient to elicit male aggressive displays

Forced activation of VMHvl^{PR} neurons triggers or intensifies aggression,[10,12] and we tested whether activating aggression-mirroring VMHvl neurons would lead to similar outcomes. We expressed the excitatory chemogenetic actuator DREADDq in VMHvl cells of TRAP2 males using aggression mirror-TRAP and tested them subsequently as single-housed residents in assays of territorial aggression and mating (Figures 7A, 7B, S7B, and S7C). Residents administered CNO were significantly more aggressive toward intruder males (Figures 7C–7G). Residents showed a ~3-fold increase in attack number, an increase that cannot be accounted for simply by the shorter latency to initiate attacks. Activation of aggression mirror-TRAPed VMHvl neurons also reduced chemoinvestigation of intruders (Figure S7A). This suggests that activation of VMHvl mirror cells reduced the need for pheromone sensing, which is otherwise essential for aggression. Activating male VMHvl^{PR} neurons also bypasses pheromonal cues emanating from females such that these males attack females rather than mating with them.[10,12] We therefore tested whether activating aggression-mirroring VMHvl neurons would alter sexual behavior with females (Figure S7C). Forced activation of these cells reduced both the probability and intensity of male sexual behavior (Figure S7D). There was a >4-fold diminution in percent of males who mounted females, loss of intromission (penetration), and reduction in mounting episodes (Figures S7E–S7H). Rather than mating with females, CNO-administered males attacked them and tail-rattled in a manner reminiscent of territorial aggression toward males (Figures S7D–S7H). Our findings demonstrate that activating aggression-mirroring VMHvl neurons intensifies male territorial aggression and supplants male sexual behavior with aggression.

Given the critical role of visual input in the mirroring properties of VMHvl neurons, we tested whether forced activation of these cells would elicit aggressive displays by mice toward their own image in a mirror. We expressed DREADDq in observer VMHvl neurons using aggression mirror-TRAP and tested the males as singly housed residents with a mirror (Figures 7H and S7I). Males administered CNO showed heightened aggressivity to the mirror, with a ~3-fold increase in the likelihood of tail-rattling and a ~10-fold increase in the number of tail-rattles (Figure 7I). These males did not attack the mirror, indicating that other sensory or contextual cues are required to trigger physical attacks, in accord with our previous findings.[10] Together, our findings demonstrate that aggression-mirroring VMHvl neurons can drive aggressive displays toward males, females, and the mouse's own mirror image.

DISCUSSION

We have identified mirror neurons for aggression. These cells reside in the nucleus of Cajal, a hypothalamic region referred to as an "attack center" for the past several decades. We demonstrate that this center represents a more abstract percept of aggression, one that evokes an aggressive state in self and reflects such a state in others. This region has been referred to as an attack center in large part because, with rare exceptions, the activity of these neurons, as well as their function, has been studied in a context in which the animal is able to initiate offensive aggression. Our study demonstrates that it is critical to record activity and perform functional interrogation of neurons in diverse settings to understand how they contribute to behavioral output. More broadly, our work answers long-standing questions about the functional contribution of mirror neurons to ongoing behavior.[28,40] We find that aggression-mirroring neurons are essential for naturally occurring territorial aggression and sufficient to elicit aggression more intensely toward males and toward atypical targets such as females and inanimate objects. Our genetic platform sets the stage for gaining molecular and cellular insights into how individual neurons co-represent higher cognitive functions such as mirroring an action and performance of that action by self.

VMHvl^{PR} neurons as mirroring neurons

The caudomedial hypothalamus has long been considered to be an attack center in diverse species, ranging from mice to humans.[3,41] Genetically targeted gain- and loss-of-function studies in mice have pinpointed VMHvl^{PR} neurons as constituting the attack center in this hypothalamic region.[9,10,12] We show that VMHvl^{PR} neurons play a more general role in aggression than previously imagined. Rather than merely modulating aggressive displays by self, these cells also appear to provide a report to self about fights between other individuals. Diverse functions, including action-understanding, sensorimotor learning such as occurs in mimicking, social cognition, cultural evolution, and art appreciation have been proposed for human mirror neuron systems.[28,40,42–51] It has been challenging to precisely test the role of mirror neurons in non-human primates, let alone humans, because they are inter-mingled with other cells and their molecular identity remains unknown. Their specific functional contributions to behavior therefore remain to be characterized in primates. The genetic tractability of the mouse has enabled us to uncover mirror neurons for aggression and show that they regulate aggression. We speculate that aggression-mirroring in mice could potentially serve one or more additional roles in the wild. Rodents exhibit empathy or consolation-type behavior toward conspecifics.[52–54] Aggressive interactions are stressful, and VMHvl^{PR} observer neurons may modulate displays of empathy or consolation-type behaviors, for example, by inhibiting them if the self is threatened or allowing them otherwise. Alternatively, aggression-mirroring may enable observers to make transitive inferences about dominance hierarchies among conspecifics. Such deductive reasoning is used by male cichlids to choose to be in proximity with weaker, lower-ranked males over dominant ones.[55] This is presumably adaptive because the observer is unlikely to be attacked by, or lose an aggressive interaction

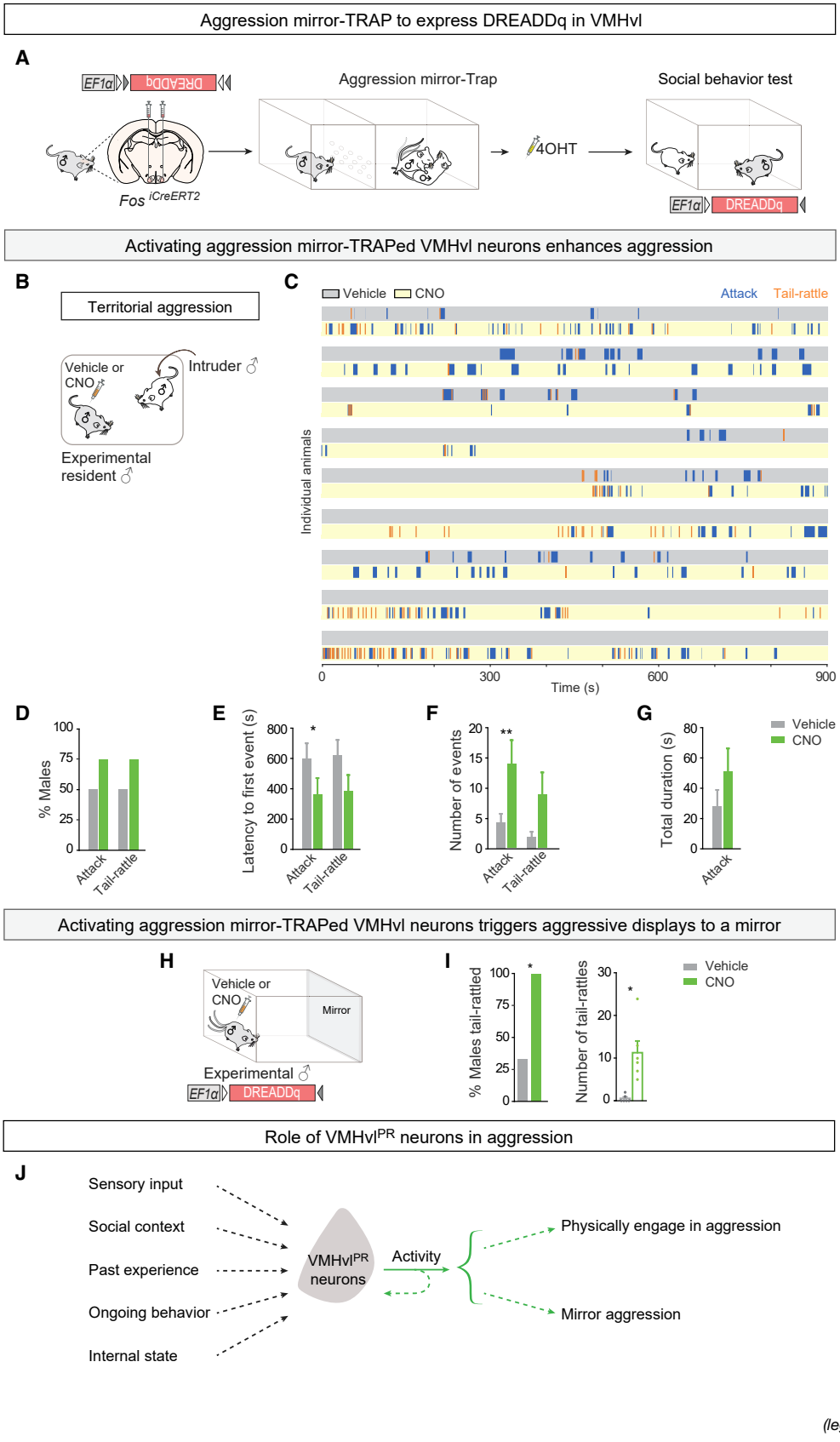

(legend on next page)

with, the weaker male. Given the immense popularity of violent video games and competitive fighting events, it appears that aggression, even if experienced vicariously, may be rewarding. Indeed, aggression is rewarding to mice, and VMHvl neurons enable operant learning for aggression-seeking behavior.[56] It will be interesting to test whether VMHvl^{PR} observer neurons are essential for aggression-related reward. Such a function might potentially underpin active seeking of vicarious aggressive experiences through gaming or spectatorship. Mice and other animals get better at fighting with prior experience or training,[21–23] but the underlying sensorimotor mechanisms remain poorly understood. It is possible that aggression-mirroring improves performance in subsequent fights or may even enable the observer to be more aggressive subsequent to witnessing a fight. Consistent with this notion, boxers may be able to better anticipate moves by opponents after viewing videos of their opponents fighting.[57] Beyond such speculation, the experimental tractability of VMHvl^{PR} neurons should enable determinination of how aggression-mirroring modulates behavior.

Consistent with the idea that aggression-mirroring VMHvl^{PR} neurons may regulate diverse behavioral outcomes, the overlap between observer and aggressor neurons is not complete. We intuit this to mean that observer neurons may overlap with other VMHvl^{PR} neurons that are activated in different contexts, such as when the mouse is the recipient of attacks by, or taking evasive action from, dominant males.[10,58,59] In other words, VMHvl^{PR} neurons may be functionally heterogeneous with regards to aggression-related behaviors and contexts, a notion consistent with the considerable molecular heterogeneity of this population.[20,35] Alternatively, the incomplete overlap between observer and aggressor neurons may reflect stochastic or more complex activation patterns of this population. We note that the activity of observer and aggressor neurons exhibits distinct dynamics during attacks. Each attack episode usually consists of a unique mix of differently evolving motor actions. One potential mechanism underlying the distinct dynamics of aggressor and observer neurons could be that the activity of the former reflects attack episodes with greater fidelity than that of the latter. For example, the activity of observer neurons may not distinguish differences in motor actions or their evolution across attack episodes such that observation effectively reflects a simplified version of the reality. Consistent with this notion, observer neurons do not appear to report non-aggressive interactions such as sniffing or grooming, behaviors that elicit reliable responses in aggressor neurons. How aggression-mirroring properties arise in VMHvl^{PR} neurons and guide behavior will be greatly informed by understanding their presynaptic partners and projection targets. BNST neurons are essential for fighting and they project to the VMHvl,[18,19,60] but they do not mirror aggression. Thus, observer cells for fighting are not present at all nodes within neural circuits that modulate this behavior. Although visual input is essential for aggression-mirroring by VMHvl^{PR} neurons, these cells do not appear to receive direct inputs from classically defined visual centers, indicating that such input occurs via a multi-synaptic relay.

In summary, we find that VMHvl^{PR} neurons constitute much more than an attack center. Our current findings with more recent work suggest a model in which VMHvl^{PR} neurons encode an agonistic state that, depending on prior experience, current social context, physiological state, and sensory cues, enables offensive or defensive aggressive responses[10,58,59]; furthermore, aggression-mirroring may endow VMHvl^{PR} neurons with additional behavioral functions as discussed above (Figure 7J). In such a model, the activity of VMHvl^{PR} neurons may not always provide a direct readout of the likelihood to initiate aggression, but rather provides a measure of an agonistic state that modulates behavioral output in an internal and external state-contingent manner.

Evolution of mirror neurons

Mirror neurons have largely been studied in the context of acquisition and improvement of learned motor skills. In contrast to such cells, the aggression-mirroring neurons we have discovered represent an innate behavioral program, and they are located in a brain region conserved across vertebrates. This suggests an ancient evolutionary origin of mirror neurons such that their original role may have been to enhance territorial defense and, ultimately, reproductive success. Our discovery of aggression-mirroring neurons raises the possibility that mirroring is also built-in into neural circuits underlying other primal behaviors such as mating and parenting. This would be consistent with the notion that one function of mirror neurons may be to support social cognition. Such a wide-ranging social mirror network could potentially provide an animal with invaluable insights into traits such as fitness, vulnerability, and social and

Figure 7. Activation of aggression-mirroring VMHvl neurons increases aggressivity

(A) Schematic of aggression mirror-TRAP strategy to express the excitatory chemogenetic actuator DREADDq in VMHvl neurons.

(B) Schematic of resident-intruder test of territorial aggression, with the aggression mirror-TRAPed resident male expressing DREADDq in VMHvl cells.

(C) Rasters of individual resident males exhibiting increased aggressivity upon chemogenetic activation of aggression-mirroring VMHvl neurons.

(D–G) Activation of aggression-mirroring VMHvl neurons did not significantly increase likelihood of initiating attacks or tail-rattles (D), but it reduced the latency to start attacking (E) and increased the number of attacks inflicted upon the intruder male (F). Other parameters of attack and tail-rattles were unaltered (E)–(G).

(H and I) Activation of aggression-mirroring VMHvl neurons increases tail-rattling to a mirror. Schematic of aggression mirror-TRAPed resident male expressing DREADDq in VMHvl neurons with a mirror in his cage (H). Activation of aggression-mirroring VMHvl neurons increased the likelihood of tail-rattling ~3-fold and the number of tail-rattles ~10-fold (I).

(J) Schematic of working model of how the activity of VMHvl^{PR} neurons may reflect agonistic states. VMHvl^{PR} neurons are sensitive to inputs from diverse, potentially inter-related sources of information, and their activity can drive physical acts of aggression (offensive or defensive) or reflect aggression-mirroring. Dashed arrows indicate that input to or output from VMHvl^{PR} neurons may occur via a multi-synaptic relay, and curved dashed arrow depicts the possibility that there may be cross-talk between VMHvl^{PR} neurons directly or via local interneurons.

Mean ± SEM n = 12 (B)–(G) and 6 (H) and (I) *Fos*^{iCreERT2} males. *p < 0.05, **p < 0.01.

See also Figure S7.

reproductive status of conspecifics in its vicinity. Intriguingly, virgin females can learn parenting from co-habiting dams,[61] although it is unclear whether such learning is supported by a corresponding mirror pathway for nursing. Invertebrate species also engage in highly elaborate social interactions, and mirror neuron systems for aggression and other social behaviors may well exist in these animals. In summary, we have discovered mirror neurons for aggression in a deeply conserved vertebrate brain region that are necessary and sufficient to elicit male territorial aggression.

Limitations of the study

We have suggested some additional roles for aggression-mirroring neurons, but it is possible that these cells do not serve other functions beyond mirroring or modulating aggression. VMHvl^{PR} neurons of males who were not previously tested for mating or territorial aggression mirror aggression. Given that these males were raised with other males post-weaning, we cannot exclude the possibility that they had fought with cage-mates or observed them fighting. We did not observe overt aggressive displays in observers that would match those being played out by demonstrators. However, observers may experience other behavioral or physiological changes, such as changes in muscle tone or titers of adrenaline or stress hormones, when viewing aggression. We have provided multiple lines of evidence showing a critical role for visual input in eliciting mirroring activity of VMHvl^{PR} neurons (Figures 2D–2F, S2M–S2N, and 7H–7I). Additional studies will reveal whether visual cues alone are sufficient to evoke mirroring. TRAP labels a subset of activated or Fos-expressing neurons following behavior.[13,37] Such under-sampling can limit full delineation of the functionality of aggression-mirroring neurons. We have used a calcium sensor to discover and characterize aggression-mirroring activity. Recording electrical activity of such aggression-mirroring neurons will afford a higher temporal resolution of the activation of these cells.

STAR★METHODS

Detailed methods are provided in the online version of this paper and include the following:

- KEY RESOURCES TABLE
- RESOURCE AVAILABILITY
  - Lead contact
  - Materials availability
  - Data and code availability
- EXPERIMENTAL MODEL AND SUBJECT DETAILS
  - Animals
  - Viruses
- METHOD DETAILS
  - Stereotaxic surgeries
  - Histology
  - Drugs
  - TRAP2 studies
  - Behavioral assays
  - Fiber photometry
  - Miniscope calcium imaging
- QUANTIFICATION AND STATISTICAL ANALYSIS

SUPPLEMENTAL INFORMATION

Supplemental information can be found online at https://doi.org/10.1016/j.cell.2023.01.022.

ACKNOWLEDGMENTS

We thank Richard Axel, Tom Clandinin, Karl Deisseroth, Lisa Giocomo, and Luis de Lecea for helpful suggestions or comments on the manuscript, Shah lab members for discussions and feedback, and Lily Duong for administrative support. This work was supported by grants to L.A.D. (Whitehall grant 2019-12-43, Klingenstein Simons Fellowship in Neuroscience), S.D. (Simons Collaboration on the Global Brain #542969; McKnight Foundation), D.L. (Ben Barres postdoctoral fellowship), L.L. (NIH R01NS050835), I.M.M. (PhD scholarship SFRH/BD/51715, Fundação para a Ciência e a Tecnologia), N.M.S. (NIH R01NS049488, R01HD109519), Y. Wei (Stanford SoM Dean's Fellowship), and T.Y. (NARSAD Young Investigator award).

AUTHOR CONTRIBUTIONS

Conceptualization, T.Y. and N.M.S.; methodology, I.M.M., Y. Wei, T.Y., and N.M.S.; software, I.M.M. and T.Y.; formal analysis, S.D., Y. Wei, and T.Y.; investigation, D.W.B., D.L., Y. Wang, Y. Wei, and T.Y.; reagents, L.A.D. and L.L.; writing, T.Y. and N.M.S.; review and editing, D.W.B., L.A.D., D.L., L.L., Y. Wei, T.Y., and N.M.S.; visualization, T.Y. and N.M.S.; supervision, L.L., T.Y., and N.M.S.; funding, L.A.D., S.D., D.L., L.L., I.M.M., T.Y., Y. Wei, and N.M.S.

DECLARATION OF INTERESTS

L.L. is a member of the advisory board for *Cell*.

INCLUSION AND DIVERSITY

One or more of the authors of this paper self-identifies as an underrepresented ethnic minority in their field of research or within their geographical location. One or more of the authors of this paper self-identifies as living with a disability. One or more of the authors of this paper received support from a program designed to increase minority representation in their field of research. While citing references scientifically relevant for this work, we also actively worked to promote gender balance in our reference list.

Received: September 21, 2022
Revised: December 13, 2022
Accepted: January 17, 2023
Published: February 15, 2023

REFERENCES

1. Gallese, V., Fadiga, L., Fogassi, L., and Rizzolatti, G. (1996). Action recognition in the premotor cortex. Brain *119*, 593–609. https://doi.org/10.1093/brain/119.2.593.
2. di Pellegrino, G., Fadiga, L., Fogassi, L., Gallese, V., and Rizzolatti, G. (1992). Understanding motor events: a neurophysiological study. Exp. Brain Res. *91*, 176–180. https://doi.org/10.1007/BF00230027.
3. Swaab, D. (2003). The ventromedial nucleus (VMN; nucleus of Cajal). In The Human Hypothalamus: Basic and Clinical Aspects Part I: Nuclei of the Human Hypothalamus (Elsevier), pp. 239–242.
4. Hess, W.R., and Akert, K. (1955). Experimental data on role of hypothalamus in mechanism of emotional behavior. AMA. Arch. Neurol. Psych. *73*, 127–129.
5. Kruk, M.R. (1991). Ethology and pharmacology of hypothalamic aggression in the rat. Neurosci. Biobehav. Rev. *15*, 527–538.
6. Kruk, M.R., van der Poel, A.M., and de Vos-Frerichs, T.P. (1979). The induction of aggressive behaviour by electrical stimulation in the hypothalamus of male rats. Behaviour *70*, 292–322.

7. Lin, D., Boyle, M.P., Dollar, P., Lee, H., Lein, E.S., Perona, P., and Anderson, D.J. (2011). Functional identification of an aggression locus in the mouse hypothalamus. Nature *470*, 221–226. https://doi.org/10.1038/nature09736.

8. Olivier, B., and Wiepkema, P.R. (1974). Behaviour changes in mice following electrolytic lesions in the median hypothalamus. Brain Res. *65*, 521–524.

9. Yang, C.F., Chiang, M.C., Gray, D.C., Prabhakaran, M., Alvarado, M., Juntti, S.A., Unger, E.K., Wells, J.A., and Shah, N.M. (2013). Sexually dimorphic neurons in the ventromedial hypothalamus govern mating in both sexes and aggression in males. Cell *153*, 896–909. https://doi.org/10.1016/j.cell.2013.04.017.

10. Yang, T., Yang, C.F., Chizari, M.D., Maheswaranathan, N., Burke, K.J., Borius, M., Inoue, S., Chiang, M.C., Bender, K.J., Ganguli, S., and Shah, N.M. (2017). Social control of hypothalamus-mediated male aggression. Neuron *95*, 955–970.e4. https://doi.org/10.1016/j.neuron.2017.06.046.

11. Falkner, A.L., Dollar, P., Perona, P., Anderson, D.J., and Lin, D. (2014). Decoding Ventromedial Hypothalamic Neural Activity during Male Mouse Aggression. J. Neurosci. *34*, 5971–5984. https://doi.org/10.1523/JNEUROSCI.5109-13.2014.

12. Lee, H., Kim, D.-W., Remedios, R., Anthony, T.E., Chang, A., Madisen, L., Zeng, H., and Anderson, D.J. (2014). Scalable control of mounting and attack by Esr1 + neurons in the ventromedial hypothalamus. Nature *509*, 627–632. https://doi.org/10.1038/nature13169.

13. DeNardo, L.A., Liu, C.D., Allen, W.E., Adams, E.L., Friedmann, D., Fu, L., Guenthner, C.J., Tessier-Lavigne, M., and Luo, L. (2019). Temporal evolution of cortical ensembles promoting remote memory retrieval. Nat. Neurosci. *22*, 460–469. https://doi.org/10.1038/s41593-018-0318-7.

14. Chen, T.-W., Wardill, T.J., Sun, Y., Pulver, S.R., Renninger, S.L., Baohan, A., Schreiter, E.R., Kerr, R.A., Orger, M.B., Jayaraman, V., et al. (2013). Ultrasensitive fluorescent proteins for imaging neuronal activity. Nature *499*, 295–300. https://doi.org/10.1038/nature12354.

15. Cui, G., Jun, S.B., Jin, X., Pham, M.D., Vogel, S.S., Lovinger, D.M., and Costa, R.M. (2013). Concurrent activation of striatal direct and indirect pathways during action initiation. Nature *494*, 238–242. https://doi.org/10.1038/nature11846.

16. Gunaydin, L.A., Grosenick, L., Finkelstein, J.C., Kauvar, I.V., Fenno, L.E., Adhikari, A., Lammel, S., Mirzabekov, J.J., Airan, R.D., Zalocusky, K.A., et al. (2014). Natural neural projection dynamics underlying social behavior. Cell *157*, 1535–1551. https://doi.org/10.1016/j.cell.2014.05.017.

17. Remedios, R., Kennedy, A., Zelikowsky, M., Grewe, B.F., Schnitzer, M.J., and Anderson, D.J. (2017). Social behaviour shapes hypothalamic neural ensemble representations of conspecific sex. Nature *550*, 388–392. https://doi.org/10.1038/nature23885.

18. Bayless, D.W., Yang, T., Mason, M.M., Susanto, A.A.T., Lobdell, A., and Shah, N.M. (2019). Limbic neurons shape sex recognition and social behavior in sexually naive males. Cell *176*, 1190–1205.e20. https://doi.org/10.1016/j.cell.2018.12.041.

19. Yang, B., Karigo, T., and Anderson, D.J. (2022). Transformations of neural representations in a social behaviour network. Nature *608*, 741–749. https://doi.org/10.1038/s41586-022-05057-6.

20. Knoedler, J.R., Inoue, S., Bayless, D.W., Yang, T., Tantry, A., Davis, C.H., Leung, N.Y., Parthasarathy, S., Wang, G., Alvarado, M., et al. (2022). A functional cellular framework for sex and estrous cycle-dependent gene expression and behavior. Cell *185*, 654–671.e22. https://doi.org/10.1016/j.cell.2021.12.031.

21. Itakura, T., Murata, K., Miyamichi, K., Ishii, K.K., Yoshihara, Y., and Touhara, K. (2022). A single vomeronasal receptor promotes intermale aggression through dedicated hypothalamic neurons. Neuron *110*, 2455–2469.e8. https://doi.org/10.1016/j.neuron.2022.05.002.

22. Juntti, S.A., Tollkuhn, J., Wu, M.V., Fraser, E.J., Soderborg, T., Tan, S., Honda, S.-I., Harada, N., and Shah, N.M. (2010). The androgen receptor governs the execution, but not programming, of male sexual and territorial behaviors. Neuron *66*, 260–272. https://doi.org/10.1016/j.neuron.2010.03.024.

23. Stagkourakis, S., Spigolon, G., Williams, P., Protzmann, J., Fisone, G., and Broberger, C. (2018). A neural network for intermale aggression to establish social hierarchy. Nat. Neurosci. *21*, 834–842. https://doi.org/10.1038/s41593-018-0153-x.

24. Leypold, B.G., Yu, C.R., Leinders-Zufall, T., Kim, M.M., Zufall, F., and Axel, R. (2002). Altered sexual and social behaviors in trp2 mutant mice. Proc. Natl. Acad. Sci. USA *99*, 6376–6381. https://doi.org/10.1073/pnas.082127599.

25. Stowers, L., Holy, T.E., Meister, M., Dulac, C., and Koentges, G. (2002). Loss of sex discrimination and male-male aggression in mice deficient for TRP2. Science *295*, 1493–1500. https://doi.org/10.1126/science.1069259.

26. Mandiyan, V.S., Coats, J.K., and Shah, N.M. (2005). Deficits in sexual and aggressive behaviors in Cnga2 mutant mice. Nat. Neurosci. *8*, 1660–1662. https://doi.org/10.1038/nn1589.

27. Yoon, H., Enquist, L.W., and Dulac, C. (2005). Olfactory inputs to hypothalamic neurons controlling reproduction and fertility. Cell *123*, 669–682. https://doi.org/10.1016/j.cell.2005.08.039.

28. Rizzolatti, G., Sinigaglia, C., and Anderson, F. (2008). Mirrors in the Brain: How Our Minds Share Actions and Emotions (Oxford University Press).

29. Aharoni, D., Khakh, B.S., Silva, A.J., and Golshani, P. (2019). All the light that we can see: a new era in miniaturized microscopy. Nat. Methods *16*, 11–13. https://doi.org/10.1038/s41592-018-0266-x.

30. Liang, B., Zhang, L., Barbera, G., Fang, W., Zhang, J., Chen, X., Chen, R., Li, Y., and Lin, D.-T. (2018). Distinct and dynamic ON and OFF neural ensembles in the prefrontal cortex code social exploration. Neuron *100*, 700–714.e9. https://doi.org/10.1016/j.neuron.2018.08.043.

31. Ziv, Y., Burns, L.D., Cocker, E.D., Hamel, E.O., Ghosh, K.K., Kitch, L.J., El Gamal, A., and Schnitzer, M.J. (2013). Long-term dynamics of CA1 hippocampal place codes. Nat. Neurosci. *16*, 264–266. https://doi.org/10.1038/nn.3329.

32. Zhou, P., Resendez, S.L., Rodriguez-Romaguera, J., Jimenez, J.C., Neufeld, S.Q., Giovannucci, A., Friedrich, J., Pnevmatikakis, E.A., Stuber, G.D., Hen, R., et al. (2018). Efficient and accurate extraction of in vivo calcium signals from microendoscopic video data. Elife *7*, e28728. https://doi.org/10.7554/eLife.28728.

33. Legaria, A.A., Matikainen-Ankney, B.A., Yang, B., Ahanonu, B., Licholai, J.A., Parker, J.G., and Kravitz, A.V. (2022). Fiber photometry in striatum reflects primarily nonsomatic changes in calcium. Nat. Neurosci. *25*, 1124–1128. https://doi.org/10.1038/s41593-022-01152-z.

34. Rizzolatti, G., and Sinigaglia, C. (2010). The functional role of the parieto-frontal mirror circuit: interpretations and misinterpretations. Nat. Rev. Neurosci. *11*, 264–274. https://doi.org/10.1038/nrn2805.

35. Kim, D.-W., Yao, Z., Graybuck, L.T., Kim, T.K., Nguyen, T.N., Smith, K.A., Fong, O., Yi, L., Koulena, N., Pierson, N., et al. (2019). Multimodal analysis of cell types in a hypothalamic node controlling social behavior. Cell *179*, 713–728.e17. https://doi.org/10.1016/j.cell.2019.09.020.

36. Krause, W.C., and Ingraham, H.A. (2017). Origins and Functions of the Ventrolateral VMH: A Complex Neuronal Cluster Orchestrating Sex Differences in Metabolism and Behavior. Adv. Exp. Med. Biol. *1043*, 199–213. https://doi.org/10.1007/978-3-319-70178-3_10.

37. Allen, W.E., DeNardo, L.A., Chen, M.Z., Liu, C.D., Loh, K.M., Fenno, L.E., Ramakrishnan, C., Deisseroth, K., and Luo, L. (2017). Thirst-associated preoptic neurons encode an aversive motivational drive. Science *357*, 1149–1155. https://doi.org/10.1126/science.aan6747.

38. Madisen, L., Zwingman, T.A., Sunkin, S.M., Oh, S.W., Zariwala, H.A., Gu, H., Ng, L.L., Palmiter, R.D., Hawrylycz, M.J., Jones, A.R., et al. (2010). A robust and high-throughput Cre reporting and characterization system for the whole mouse brain. Nat. Neurosci. *13*, 133–140. https://doi.org/10.1038/nn.2467.

39. Roth, B.L. (2016). DREADDs for neuroscientists. Neuron *89*, 683–694. https://doi.org/10.1016/j.neuron.2016.01.040.

40. Heyes, C., and Catmur, C. (2022). What happened to mirror neurons? Perspect. Psychol. Sci. *17*, 153–168. https://doi.org/10.1177/1745691621990638.

41. Reeves, A.G., and Plum, F. (1969). Hyperphagia, rage, and dementia accompanying a ventromedial hypothalamic neoplasm. Arch. Neurol. *20*, 616–624.

42. Gallese, V., Keysers, C., and Rizzolatti, G. (2004). A unifying view of the basis of social cognition. Trends Cogn. Sci. *8*, 396–403. https://doi.org/10.1016/j.tics.2004.07.002.

43. Heyes, C. (2013). A new approach to mirror neurons: developmental history, system-level theory and intervention experiments. Cortex *49*, 2946–2948. https://doi.org/10.1016/j.cortex.2013.07.002.

44. Oberman, L.M., Pineda, J.A., and Ramachandran, V.S. (2007). The human mirror neuron system: A link between action observation and social skills. Soc. Cogn. Affect. Neurosci. *2*, 62–66. https://doi.org/10.1093/scan/nsl022.

45. Prather, J.F., Peters, S., Nowicki, S., and Mooney, R. (2008). Precise auditory–vocal mirroring in neurons for learned vocal communication. Nature *451*, 305–310. https://doi.org/10.1038/nature06492.

46. Ramachandran, V.S. (2000). Mirror Neurons and Imitation Learning as the Driving Force behind "The Great Leap Forward" in Human Evolution (Edge).

47. Dumitrescu I. Physical, Cultural, Personal: The Demands of Dance. TLS. February 1, 2019. #6044.

48. Bell J. Work from Life. TLS. March 27, 2020. #6104.

49. Vogeley, K. (2017). Two social brains: neural mechanisms of intersubjectivity. Philos. Trans. R. Soc. Lond. B Biol. Sci. *372*, 20160245. https://doi.org/10.1098/rstb.2016.0245.

50. Gallese, V., Gernsbacher, M.A., Heyes, C., Hickok, G., and Iacoboni, M. (2011). Mirror Neuron Forum. Perspect. Psychol. Sci. *6*, 369–407. https://doi.org/10.1177/1745691611413392.

51. Hickok, G., and Hauser, M. (2010). Mis)understanding mirror neurons. Curr. Biol. *20*, R593–R594. https://doi.org/10.1016/j.cub.2010.05.047.

52. Burkett, J.P., Andari, E., Johnson, Z.V., Curry, D.C., de Waal, F.B.M., and Young, L.J. (2016). Oxytocin-dependent consolation behavior in rodents. Science *351*, 375–378. https://doi.org/10.1126/science.aac4785.

53. Schaich Borg, J., Srivastava, S., Lin, L., Heffner, J., Dunson, D., Dzirasa, K., and de Lecea, L. (2017). Rat intersubjective decisions are encoded by frequency-specific oscillatory contexts. Brain Behav. *7*, e00710. https://doi.org/10.1002/brb3.710.

54. Smith, M.L., Asada, N., and Malenka, R.C. (2021). Anterior cingulate inputs to nucleus accumbens control the social transfer of pain and analgesia. Science *371*, 153–159. https://doi.org/10.1126/science.abe3040.

55. Grosenick, L., Clement, T.S., and Fernald, R.D. (2007). Fish can infer social rank by observation alone. Nature *445*, 429–432. https://doi.org/10.1038/nature05511.

56. Falkner, A.L., Grosenick, L., Davidson, T.J., Deisseroth, K., and Lin, D. (2016). Hypothalamic control of male aggression-seeking behavior. Nat. Neurosci. *19*, 596–604. https://doi.org/10.1038/nn.4264.

57. Skoghagen, L., and Andersson, L. (2022). The integration of contextual priors and kinematic information during anticipation in skilled boxers : The role of video analysis (School of Health and Welfare, Halmstad University).

58. Krzywkowski, P., Penna, B., and Gross, C.T. (2020). Dynamic encoding of social threat and spatial context in the hypothalamus. Elife *9*, e57148. https://doi.org/10.7554/eLife.57148.

59. Sakurai, K., Zhao, S., Takatoh, J., Rodriguez, E., Lu, J., Leavitt, A.D., Fu, M., Han, B.-X., and Wang, F. (2016). Capturing and manipulating activated neuronal ensembles with CANE delineates a hypothalamic social-fear circuit. Neuron *92*, 739–753. https://doi.org/10.1016/j.neuron.2016.10.015.

60. Lo, L., Yao, S., Kim, D.-W., Cetin, A., Harris, J., Zeng, H., Anderson, D.J., and Weissbourd, B. (2019). Connectional architecture of a mouse hypothalamic circuit node controlling social behavior. Proc. Natl. Acad. Sci. USA *116*, 7503–7512. https://doi.org/10.1073/pnas.1817503116.

61. Carcea, I., Caraballo, N.L., Marlin, B.J., Ooyama, R., Riceberg, J.S., Mendoza Navarro, J.M., Opendak, M., Diaz, V.E., Schuster, L., Alvarado Torres, M.I., et al. (2021). Oxytocin neurons enable social transmission of maternal behaviour. Nature *596*, 553–557. https://doi.org/10.1038/s41586-021-03814-7.

62. Harris, J.A., Hirokawa, K.E., Sorensen, S.A., Gu, H., Mills, M., Ng, L.L., Bohn, P., Mortrud, M., Ouellette, B., Kidney, J., et al. (2014). Anatomical characterization of Cre driver mice for neural circuit mapping and manipulation. Front. Neural Circuits *8*, 76. https://doi.org/10.3389/fncir.2014.00076.

63. Inoue, S., Yang, R., Tantry, A., Davis, C.-H., Yang, T., Knoedler, J.R., Wei, Y., Adams, E.L., Thombare, S., Golf, S.R., et al. (2019). Periodic remodeling in a neural circuit governs timing of female sexual behavior. Cell *179*, 1393–1408.e16. https://doi.org/10.1016/j.cell.2019.10.025.

64. Wu, M.V., Manoli, D.S., Fraser, E.J., Coats, J.K., Tollkuhn, J., Honda, S.-I., Harada, N., and Shah, N.M. (2009). Estrogen masculinizes neural pathways and sex-specific behaviors. Cell *139*, 61–72. https://doi.org/10.1016/j.cell.2009.07.036.

STAR★METHODS

KEY RESOURCES TABLE

REAGENT or RESOURCE	SOURCE	IDENTIFIER
Antibodies		
Sheep anti-GFP	Biorad	Cat # 4745-1051; RRID: AB_619712
Rat anti-RFP	Chromotek	Cat # 5f8-100; RRID: AB_2336064
Rabbit anti-Fos	EMD Millipore	Cat # PC38; RRID: AB_2106755
Rabbit anti-Esr1	Millipore	Cat #: 06-935; RRID: AB_310305
Donkey anti-sheep, Alexa 488 Conjugate	Jackson ImmunoResearch	Cat # 713-545-147; RRID: AB_2340745
Donkey anti-rat, Cy3 conjugate	Jackson ImmunoResearch	Cat # 712-165-150; RRID: AB_2340666
Donkey anti-rabbit, Cy3 conjugate	Jackson ImmunoResearch	Cat # 711-165-152; RRID: AB_2307443
Bacterial and virus strains		
Recombinant adeno-associated virus: AAV1-Syn-FLEX-GCaMP6s	Penn Vector Core	Addgene number: 100845
Recombinant adeno-associated virus: AAV1-CAG-FLEX-eGFP	Penn Vector Core	Addgene number: 59331
Recombinant adeno-associated virus: AAVDJ-EF1a-DIO-hM4D(GI)-mCherry	UNC Vector Core	Addgene number: 50461
Recombinant adeno-associated virus: AAVDJ-EF1a-DIO-hM3D(Gq)-mCherry	UNC Vector Core	Addgene number: 50460
Chemicals, peptides, and recombinant proteins		
DAPI	Sigma-Aldrich	Cat #D9542; CAS 28718-90-3
Clozapine-N-oxide (CNO)	Enzo Life Sciences	Cat # BML-NS105-0005
4-Hydroxytamoxifen	Sigma-Aldrich	Cat #H6278; CAS 68392-35-8
Estradiol	Sigma-Aldrich	Cat #E8875; CAS 50-28-2
Progesterone	Sigma-Aldrich	Cat #P0130; CAS 57-83-0
Castor oil	Sigma-Aldrich	Cat # 259853; CAS 8001-79-4
Sunflower seed oil	Sigma-Aldrich	Cat #S5007; CAS 8001-21-6
Sesame oil	Sigma-Aldrich	Cat #S3547; CAS 8008-74-0
Experimental models: Organisms/strains		
Mouse: *C57BL/6J*	The Jackson Laboratory	Stock # 000664; RRID: IMSR_JAX:000,664
Mouse: *129/SvEvTac*	Taconic Biosciences	Stock # 129SVE-M
Mouse: PR^{Cre}	Jackson Laboratories	Stock # 017915; RRID:IMSR_JAX:017,915
Mouse: $Fos^{iCreERT2}$	Jackson Laboratories	Stock # 030323; RRID:IMSR_JAX:030,323
Mouse: $Tac1^{Cre}$	Jackson Laboratories	Stock No: 021,877; RRID:IMSR_JAX:021,877
Mouse: *Ai14*	Jackson Laboratories	Stock No: 007,914; RRID:IMSR_JAX:007,914
Mouse: $Trpc2^{+/-}$	Leypold et al.[24]	N/A
Software and algorithms		
ImageJ	NIH	https://imagej.nih.gov/ij/index.html; RRID: SCR_003070
MATLAB	MathWorks	https://www.mathworks.com/products.html; RRID: SCR_001622
GraphPad Prism 6	GraphPad Software	https://www.graphpad.com/scientific-software/prism/; RRID: SCR_002798
Inscopix Data Processing Software	Inscopix Inc.	https://www.inscopix.com/software-analysis-miniscope-imaging#software_idps

RESOURCE AVAILABILITY

Lead contact

Further information and requests for resources and reagents should be directed to and will be fulfilled by the lead contact, Dr. Nirao M. Shah (nirao@stanford.edu).

Materials availability

This study did not generate new unique reagents.

Data and code availability

- Data reported in this paper will be shared by the lead contact upon request.
- All MATLAB scripts used in this manuscript are available from the lead contact upon reasonable request.
- Any additional information required to reanalyze the data reported in this paper is available from the lead contact upon request.

EXPERIMENTAL MODEL AND SUBJECT DETAILS

Animals

All mice were bred in our colony (*Ai14, Fos*^{iCreERT2}, *PR*^{Cre}, *Tac1*^{Cre}, *Trpc2*$^{-/+}$) or purchased from Jax (*C57BL/6J*, used as stimulus females in mating assays) and Taconic (*129/SvEvTac*, used as WT intruder males).[9,13,24,37,38,62] All experiments were performed on adult mice ranging from ~10 to ~20 weeks of age. *Fos*^{iCreERT2} mice of mixed C57BL/6J and 129; FVB background were back-crossed into C57BL/6J background in the lab ≥2 times prior to being used for mirror-TRAP studies. This mixed background likely resulted in differences in various behavioral parameters between experimental cohorts. Importantly, for our chemogenetic studies, vehicle and CNO were provided in a randomized manner to individual mice, thereby enabling rigorous comparison of behavioral performance ± CNO. Mice were housed under a reverse 12:12 h light:dark cycle (lights off at 1p.m.) with controlled air, temperature, and humidity, and food and water were provided *ad libitum*. All animal studies were in compliance with Institutional Animal Care and Use Committee guidelines and protocols approved by Stanford University's Administrative Panel on Laboratory Animal Care and Administrative Panel of Biosafety.

Viruses

AAV-hSyn-Flex-GCaMP6s (serotype 1) was purchased from Addgene or Penn Vector Core. AAV-EF1α-Flex-hM3Dq:mCherry (serotype DJ, encoding DREADDq) and AAV-EF1α-Flex-hM4Di:mCherry (serotype DJ, encoding DREADDi) were custom packaged by the UNC Vector Core with plasmid DNA that was originally purchased from Addgene. All virus titers were > 10^{12} genomic copies/mL. For miniscope calcium imaging, following optimization of GCaMP6s expression in soma but not nucleus with a series of virus dilutions, we used 1:20 dilution of virus stock in sterile PBS.

METHOD DETAILS

Stereotaxic surgeries

Virus was delivered to the brains of male mice at 9–16 weeks of age, using a Kopf stereotaxic alignment system (model 1900), as described previously.[10] The exposed skull was leveled anteroposteriorly between bregma and Lambda and mediolaterally between the left and right hemispheres. To deliver AAV-encoded DREADD bilaterally, a custom-prepared 33G stainless hypodermic cannula connected to a Hamilton syringe via polyethylene tubing was loaded with 1 μL of virus and infused at 100 nL/min using a syringe pump (Harvard Apparatus). To deliver AAV-encoded GCaMP6s unilaterally, a NanoFil syringe (World Precision Instruments, WPI) with a 26G beveled needle was loaded with 200 nL (miniscope) or 600 nL (fiber photometry) of virus and infused at 30 or 50 nL/min using a microinjection syringe pump (WPI). For most unilateral injections, the same hemisphere was selected per cohort of animals for the sake of consistency in surgery. When the injection was completed, the needle was left for an additional 10 min and withdrawn at 1 min/mm. To deliver viruses to the VMHvl, we used the following stereotaxic coordinates relative to bregma: anteroposterior −1.4 mm, lateral ±0.78 mm, dorsoventral −5.8 mm. To deliver viruses to the BNST, we used the following stereotaxic coordinates relative to bregma: anteroposterior −0.2 mm, lateral ±0.85 mm, dorsoventral −4.3 mm. When the distance between bregma and Lambda (BL) was larger than 4 mm, the anteroposterior coordinate was adjusted based on the fact that the BL distance is 3.8 mm in a standard adult mouse brain atlas.

To prepare for optic fiber or gradient refractive index (GRIN) lens implantation, the surface of the skull was scored with a standard 21G hypodermic needle and treated with 0.3% hydrogen peroxide. For fiber photometry imaging, a custom-made fiber optic cannula was lowered at 1 mm/min immediately after withdrawing the injection needle and placed 300 to 400 μm above the dorsoventral coordinate used for viral delivery. For miniscope imaging, a 0.6 × 7.3 mm (diameter x length) GRIN lens (Inscopix) was implanted 3 weeks after viral injection. The GRIN lens was connected to a miniscope imaging system (nVista, Inscopix), lowered at 0.5 mm/min while monitoring fluorescence, and placed between 150 and 250 μm dorsal and 90 μm medial to the coordinates

used for vial delivery. The GRIN lens was capped with a small piece of parafilm and silicon adhesive (Kwik-Sil, WPI) prior to closing the skin incision. The silicon cover was removed 10 days after GRIN lens implantation and a baseplate (Inscopix) was installed above the GRIN lens. The baseplate was connected to the miniscope, lowered until clear cellular morphology was detected across the imaging plane, anchored to the skull with adhesive, and covered with a baseplate cover (Inscopix). The cannula, GRIN lens, and baseplate were secured to the skull using adhesive dental cement (C&B Metabond, Parkell).

Histology

Expression of GCaMP6s or DREADD (mCherry-conjugated) was quantified for all experimental animals, as previously described.[10,18,20,63] Mice were anesthetized with 2.5% avertin and perfused with HBS followed by 4% paraformaldehyde (PFA). Brains were dissected, post-fixed in 4% PFA overnight, sectioned at 65μm thickness with a vibratome (Leica VT1000S), and immunolabeled and counter-stained with DAPI (0.2 μg/mL) as previously described.[10] Primary antisera were rat anti-RFP (Chromotek; 1:2000), sheep anti-GFP (BioRad; 1:2000), rabbit anti-Fos (Santa Cruz Biotechnology; 1:1000), and rabbit anti-Esr1 (Millipore; 1:10,000). Secondary antisera were Cy3 donkey anti-rat (Jackson ImmunoResearch; 1:800), Alexa Fluor 488 donkey anti-rabbit (Invitrogen; 1:300), and Alex Fluor 488 donkey anti-sheep (Jackson ImmunoResearch; 1:300). To label activated neurons during aggression or observation of aggression, brain sections were immunolabeled for Fos, as described previously.[10,18,63] In brief, following 15 min of behavioral testing (as aggressors or observers), males were returned to the home cage and perfused with 4% PFA 1 h later. We verified that CNO activated DREADDq+ neurons in a subset of experimental males because Fos was induced in these males with CNO, which was administered 1 h prior to perfusion and histological analysis. Sections were imaged using confocal microscopy (LSM800, Zeiss) and quantified using ImageJ software (NIH) as described previously.[10,18]

Drugs

4OHT (Sigma, cat# H6278) was prepared as previously described.[13,37] In brief, the stock solution was prepared by dissolving 4OHT in ethanol at 20 mg/mL by shaking and brief incubation at 55°C, and then aliquots were sealed with parafilm and stored at −20°C until use. To prepare a working solution, 4OHT in a stock aliquot was redissolved by shaking and brief incubation at 55°C and an equal volume of Chen Oil (a 1:4 mixture of castor oil: sunflower seed oil; Sigma, cat# 259853 and S5007, respectively) was added. The 4OHT-oil mixture was vortexed, briefly spun down, and incubated at 55°C on a heat block with a cap opened under a light-protective cover for about 2–3 h until ethanol had evaporated. An equal volume of Chen Oil was added to make a final, working solution of 10 mg/mL 4OHT, which was stored at 4°C and used only on the day of preparation.

CNO solution was prepared as previously described.[10] In brief, CNO (Enzo) was dissolved in sterile saline at 5 mg/mL, aliquots were frozen, and each aliquot was freshly diluted with sterile saline prior to intra-peritoneal (ip) administration. The final dose of CNO for chemogenetic studies was 3 mg/kg unless otherwise mentioned.

Females were hormonally primed as described before.[10] In brief, we injected subcutaneously 17-β-estradiol benzoate (Sigma, cat# E8515) at 10 μg in 100 μL sesame oil on day −2, 5 μg in 50 μL sesame oil on day −1, and progesterone (Sigma, cat# P0130) at 50 μg in 50 μL sesame oil on day 0, the day of the mating test. Females were used for mating 4–6 h after administration of progesterone.

TRAP2 studies

Adult *Fos*^{iCreERT2} males were injected with a Cre-dependent AAV virus encoding DREADD or GCaMP6s, singly housed for a week; these males were provided with mating experience (with a WT, receptive female) and aggression toward a WT intruder males, unless stated otherwise. For aggression-TRAP or aggression mirror-TRAP, these experimental males were allowed to attack a WT intruder in their home cage for 15 min or witness aggression between unfamiliar demonstrator males for 15 min in the observation setup. For non-aggressive interaction mirror-TRAP, experimental males witnessed interactions between Trpc2 null sibling males for 15 min in the observation setup. Observer males were then returned to their home cage. Aggressor or observer males were administered 4OHT at 50 mg/kg ip 1 h after the behavioral testing was concluded. These males were TRAPed once more 2–3 days following the first TRAPing session to maximize the number of genetically tagged neurons. Histological or behavioral studies were done 10 days after the second TRAPing procedure, whereas fiber photometry was done 3 weeks following TRAPing to ensure functional expression of GCaMP6s.

Behavioral assays

Behavioral assays were performed ≥1 h after onset of the dark cycle and recorded using either a web camera (an infrared filter manually removed) or a camcorder (Sony) under infrared illumination unless mentioned otherwise. Experimental males were group housed after weaning, underwent stereotaxic surgery, and were singly housed >10 days prior to behavioral testing. Behavioral assays were performed >10 days or >3 weeks after viral injection of DREADD or GCaMP6s, respectively, for optimal expression. Mice were never tested more than once/day, with sequential behavioral tests separated by ≥ 2 days, and experimental animals were always presented with an unfamiliar intruder in their home cage or unfamiliar demonstrators separated by a partition. Male mice were tested for mating for 30 min with a group-housed WT female (C57BL/6J) that was hormonally primed to be receptive. Subsequently, males were tested for aggression with a socially housed stimulus male (129/SvEvTac) for 15 min. For DREADD experiments, mice were tested 30 min after ip administration of either sterile vehicle (saline) or CNO. Mice were tested two days apart once each with saline and CNO, with vehicle and drug counterbalanced across animals.

An observation chamber was built using a conventional rat cage (45 × 25 × 20 cm, LxWxH), which was divided into two compartments (1:2) by inserting a perforated light-weight transparent plastic panel parallel to the short axis of the cage. Perforations were 1.27 cm diameter and spread evenly throughout the bottom third of the panel. An enclosed observation chamber was built in a similar way, except that the divider was not perforated, and the ceiling of the larger compartment was completely covered with a transparent plastic panel. Before initiation of the assay, the smaller compartment was scattered with clean bedding and the larger compartment was scattered with soiled bedding from the cage of the aggressive demonstrator. For observation of aggressive encounters between two male demonstrators, an observer was first allowed to explore the small compartment 5 min later. Then, a singly housed male demonstrator was introduced into the larger compartment, followed 5 min later with the insertion of a socially housed stimulus male (129/SvEvTac) in the same compartment. The observation of aggressive encounters persisted for 15 min. Unless otherwise mentioned, observation assays were conducted under white light illumination (~90 lux; cf. the average ambient brightness of the animal room was 290 lux during lights-on). For experiments shown in Figures 2D–2F where the observation assay was conducted with red light, we used LED bulbs (emitting 850 nm, $\leq$1 lux) pointed at the ceiling of the behavioral chamber such that the observation setup in which the animals were housed was illuminated with diffuse, reflected 850 nm light. For experiments with a running wheel, we allowed the experimental observer male to explore the smaller compartment of the observer setup for 5 min, inserted a horizontally spinning plastic wheel (18 cm diameter) into the larger compartment, and, 5 min later, placed a singly housed demonstrator male on the wheel; the assay was terminated 5 min following insertion of the demonstrator.

To ensure reliable and comparable aggression between demonstrators across multiple assays, we used two sets of demonstrators. One set of demonstrators comprised of group-housed adult WT males (129/SvEvTac) that would be reliably submissive. The other set of demonstrators comprised of singly housed adult PR^{Cre} males that expressed DREADDq in $VMHvl^{PR}$ neurons. DREADDq was encoded in a Cre-contingent AAV format and stereotaxically delivered, using coordinates described earlier, $\geq$10 days prior to using the male as a demonstrator. These males were administered CNO ip (0.3 mg/kg) 30 min prior to insertion into the demonstrator compartment. As shown before, such PR^{Cre} males are reliably aggressive toward other males.[10]

We used ovariectomized, hormonally primed, and sexually experienced females for mating assays to ensure that they were reliably receptive to mating attempts by experimental males. Adult females were ovariectomized, allowed to recover from surgery for $\geq$4 weeks, primed to be in estrus, and mated twice (separated by a week) with a sexually experienced WT male. These females were subsequently used in mating assays no more than once/week.

Fiber photometry

Fiber photometry calcium imaging was conducted as previously described.[1,63] To make a fiber optic cannula, a 400 μm core, 0.5 NA multimode optical fiber (Thorlabs, FT400URT) was stripped (Thorlabs, T18S25), lightly scored at 2 cm from the end of fiber with a carbide fiber scribe (Thorlabs, S90C), and pulled horizontally by hand. The surface at the tip of each fiber was inspected using a fiber inspection scope (Thorlabs, FS200), and each fiber with a >95% mirror-like smooth surface was inserted into a ceramic ferrule (Thorlabs, CF440) such that 8 mm of fiber with the smooth end protruded out of the ferrule. Fiber optic epoxy (Thorlabs, F120) was used to glue both ends of the ferrule to the optic fiber. The assembled cannula was cured overnight and any extra epoxy on the ferrule was removed with a razor blade. The other, non-mirrored, end of the optical fiber was cut with a fiber scribe, polished sequentially with a 3 and 0.3 μm grit lapping sheet (Thorlabs, LF3P, LF03P, D50-FC), and then inspected with a scope. Cannulas with >95% smooth surface on both ends were implanted after GCaMP6s was virally delivered. The top surface of the implanted cannula was cleaned with fiber connector cleaning fluid and stick (Thorlabs, FCS3, MCC25) and was jointed with a patch cable (home-made or purchased from RWD Life Science) via a ceramic mating sleeve (Thorlabs, ADAF1). The other side of the patch cable was connected to a custom-built fiber photometry setup, as previously described.[18,63] The excitation light emitted from a 473 nm diode laser (Omicron LuxX) passed through an optic chopper (Thorlabs, MC2000) running at 400 Hz, neutral density filters (Thorlabs NE10B-A, NE30B-A, NE50B-A), a GFP excitation filter (Thorlabs, MF369-35), a dichroic mirror (Semrock, FF495-Di03-25x36), and a fiber collimator (Thorlabs, F240FC) before being directed to a patch cable. The emitted light from GCaMP6s passed through a fiber collimator, a GFP emission filter (Thorlabs, MF525-39), and a dichroic mirror, and was focused by a plano-convex lens (Thorlabs, LA1255-A) onto a femtowatt photoreceiver (Newport, 2151). The signal from the photoreceiver was relayed to a lock-in amplifier (Stanford Research System, SR810), which also received a phase lock-in signal from the optic chopper. The output signal from the amplifier was recorded on a computer via a data acquisition device (LabJack, U6-Pro) at a 250 Hz sampling rate.

At the beginning of a photometry imaging session, a flashing red light generated by a TTL pulse generator (doric, OPTG-4) was used to synchronize annotated behaviors with fluorescence signal. Fluorescence was recorded for 5 min before introducing a stimulus in the home cage or demonstrators in the larger compartment of the observation setup. A custom code written in MATLAB and described previously was used to synchronize fluorescence signal with manually annotated behavior epochs.[18,63]

All raw fluorescence signals obtained during behavioral testing were first normalized to the median fluorescence during the 5 min period preceding the behavioral test (referred to as raw signals hereafter), and these raw signals were further processed using a moving average filter prior to any additional analysis. To visualize neuronal activity during individual behavior epochs as a heatmap, the onset of each behavior epoch was set as zero and signals between −10 and 10 s (F_t, where t denotes each time frame) were normalized to the median value (F_0) between −10 s and −5 s, such that the relative fluorescence change was calculated as $\Delta F_n = (F_t - F_0)/F_0$. We excluded data from analysis if there was an overlap of behaviors within this time window. To generate a peri-event time plot (PETP), fluorescence signals were converted into *Z* score. Mean (μ) and SD(σ) calculated from fluorescence signals

between −10 s and −5 s of the onset of a behavioral epoch were used to derive *Z* scores {*Z* score = $(F_t - \mu)/\sigma$}. These *Z* scores were averaged across all epochs per animal. The values between −10 s and −5 s of the onset of the same class of behavioral epoch from all animals were used to determine the mean and SD of baseline activity, which were then used to calculate *Z* scores to reflect the variation between individual animals. The corresponding *Z*-scored trace was used to depict the PETP. We used the mean fluorescence value between −10 s and −5 s as baseline (Base., in Figure panels) signal preceding onset of a behavioral event and 95% peak fluorescence value between 0 and 10 s was used as peak signal for that event.

Miniscope calcium imaging

We employed a miniaturized fluorescence microscopy setup (nVista, Inscopix) to perform miniscope calcium imaging. The baseplate cover was removed and a miniscope was mounted and secured with a side screw. To synchronize fluorescence signals with annotated behaviors, we used an excitation LED-triggered TTL signal generated by a data acquisition device or a camera that captured the excitation LED flash. To try to ensure reproducible imaging across sessions, we used identical LED power, lens focus, digital gain, exposure time, and recording frame rate for all sessions for the same animal.

Imaging data was loaded on Inscopix data processing software (IDPS, Inscopix) and the size of the image was cropped in a rectangular shape to cover the area of the GRIN lens. The cropped data was processed to rectify defective pixels, spatially downsampled by a factor of two to reduce data size, filtered with a spatial bandpass to remove low and high spatial frequency content, and corrected for motion so that each pixel corresponded to the same location in imaging area across all frames. To identify the spatial locations of neurons {spatial masks of identified regions of interest (ROIs)} and its associated fluorescence signal from the processed imaging data, a constrained nonnegative matrix factorization-extended (CNMF-E) algorithm was applied in MATLAB along with IDPS.[32] We used raw rather than deconvoluted signals for subsequent analyses since they displayed higher dynamics and non-artificial changes in calcium activity. Identified ROIs were further screened based on all pixels being singly connected, morphology, location in imaging field, size, dynamics of associated raw calcium signal, and signal:noise of calcium signal. Calcium signals associated with each identified ROI (neuron) were synchronized with annotated behaviors, *Z*-scored for all behavioral epochs of the same class for each ROI, using values of F_t, F_0, μ, and σ as defined for fiber photometry. To determine whether an identified ROI generated a significant response during behavior epochs, the cumulative distribution of *Z* scores between −10 and 0 s to the onset of the behavior epoch was compared with that between 0 and 10 s using Kolmogorov-Smirnov (KS) test. When the p value from the KS test was <0.05, the corresponding ROI was considered significantly responsive for a given behavior. To further understand the detail of calcium dynamics during behavior, all significantly responsive traces were grouped by the *k*-means clustering algorithm using a correlation distance metric, and this clustering process was repeated 6 times. In general, the traces for the analyzed behaviors, including attack, tail-rattle, observing attack, and observing tail-rattle, were categorized into four patterns, such as persistent activation, immediately transient activation, delayed activation, and persistent inhibition. For further analysis, these four classes of activity were grouped as either activated (including persistent, immediately transient, and delayed activation) or inhibited ROIs (KS test for activated ROIs, $p = 0.0011 \pm 0.0003$; KS test for inhibited ROIs, $p = 0.0005 \pm 0.0004$; mean ± SEM). These values corresponded to a *Z* score >1.5 and < −1.5 for all activated and inhibited ROIs shown in Figures 4, S4, 5, and S5.

To determine whether a given ROI was reliably activated or inhibited during a given behavioral class, we devised a reliability index for the two general classes of responses (activation and inhibition) described above, as follows. For a given behavioral class, reliability index = (# epochs showing activation/total # of epochs) for activation, and reliability index = (# epochs showing inhibition/total # of epochs) for inhibition. To obtain chance levels of reliability index, we shuffled the entire set of fluorescence signals per ROI using permutated time points for the duration of the behavioral assay.

Identical ROIs between imaging sessions were determined with a custom code written in MATLAB. For every animal, a reference session was selected and alignment between references and remaining sessions was done using spatial masks obtained from CNMF-E single ROI extraction. The alignment is based on a stepwise registration approach, where consecutive refined alignments between two sessions are done iteratively using thresholded ROI masks and centroid coordinates, based on previous iteration results. Reference centroid coordinates are then used as seeds for finding matching cells across registered sessions. Validation was done by setting a Euclidean distance threshold between centroids and manual inspection of spatial masks.

QUANTIFICATION AND STATISTICAL ANALYSIS

Behaviors were annotated using a software package in MATLAB as previously described.[10,64] Behavioral events scored during mating include grooming, investigation (close contact of non-anogenital regions by the nose), sniff (anogenital investigation), mounting (short, rapid thrusts), intromission (longer, slower thrusts), and ejaculation. Behavioral events scored during aggression include grooming, investigation, sniff, attack (biting, wrestling, boxing, and chasing if flanked by biting, wrestling, or boxing), and tail-rattle. We annotated mating-specific (mount, intromission, ejaculation) and aggression-specific (attack, tail-rattle) behavioral events for both mating and aggression assays. For observers (Figures S2A and S2B), we also annotated tail-rattles or sudden, rapid movements (“running events”) that could conceivably be construed as the rapid movements that naturally occur during aggression, such as chasing, when they were watching demonstrators. We annotated time points at which the observer was facing the demonstrators, and fluorescence signals for both fiber photometry and miniscope imaging were analyzed only when the observer was facing the demonstrators. In separate analyses (for Figures S2M−S2N), we analyzed fluorescence signals for fiber photometry only when

the observer was facing 180° away from the demonstrators. This allowed us to determine whether cues from other sensory modalities such as audition or chemosensation were sufficient to evoke mirroring in the absence of visual cues of aggression. Experimenters were blinded to relevant variables (including identity of administered solution, genotype, and genotype of virally encoded transgenes) during behavioral annotation and only unblinded for statistical analysis.

Statistical analysis was performed using GraphPad PRISM (GraphPad Software) or MATLAB. To compare categorical data, including the percentage of animals displaying behaviors, a two-tailed Fisher exact test was performed from a 2x2 contingency table. In the case of a male attacking a female, a one-tailed Fisher exact test was used since a male did not display attacks toward a female in a control condition. Non-categorical data, such as behavioral parameters, including the number of events, latency to the first event, and total duration of the event, or calcium signals, including mean basal activity and 95% peak amplitude after the onset of the event, were analyzed to determine if the data were normally distributed using D'Agostino-Pearson omnibus normality test. In experiments when samples were paired, a paired t test and Wilcoxon matched-pairs signed rank test were used for parametric and non-parametric data, respectively. In all other experiments, a t test, t test with Welch's correction for unequal SD were used for parametric data, and a Mann-Whitney test was used for non-parametric data. We compared activation dynamics of ROIs shown in Figures 4C, 4G, 4K, and 4O using a repeated measures-ANOVA with Šidák's multiple comparisons test.

Supplemental figures

CellPress
OPEN ACCESS

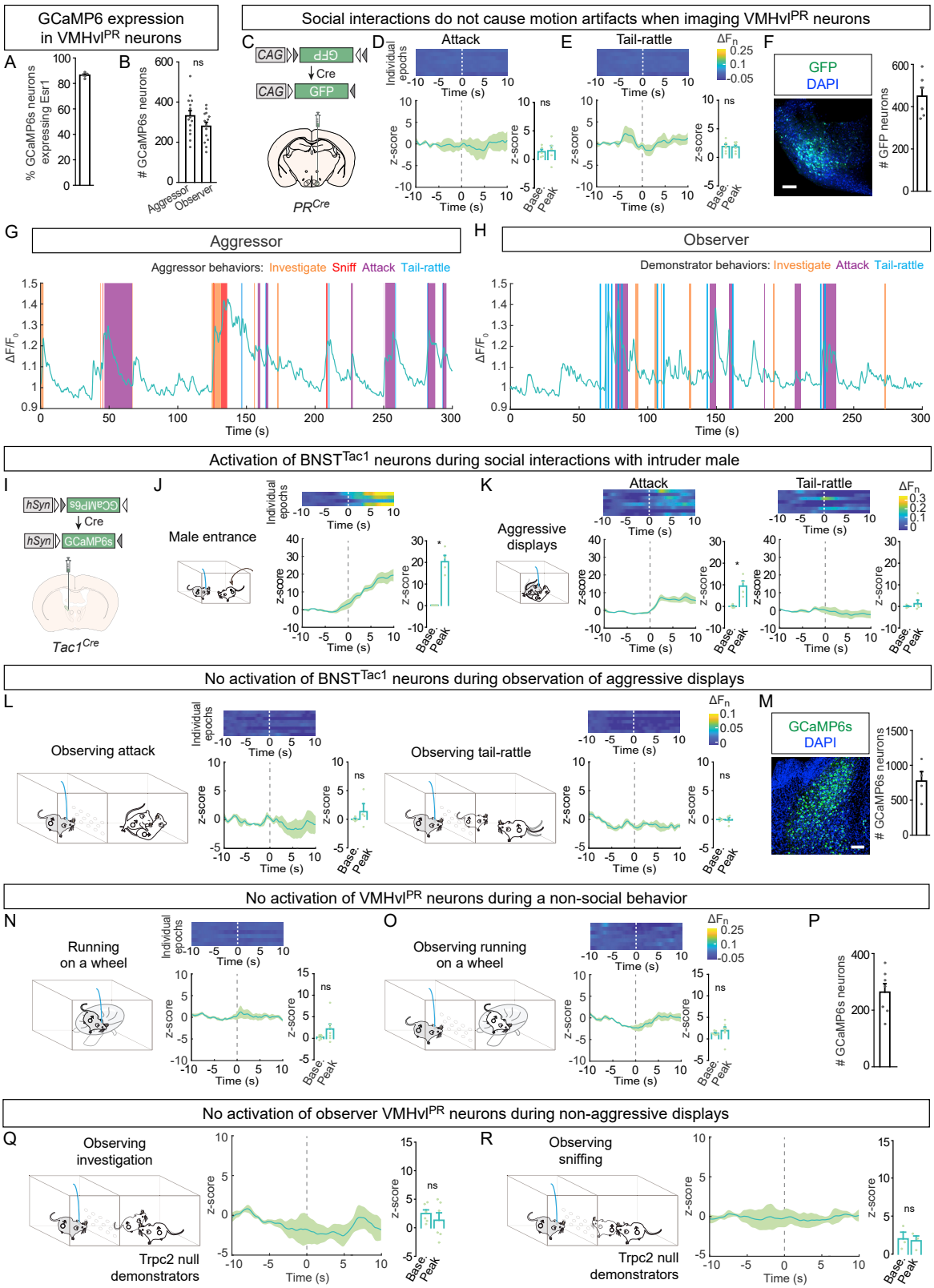

(legend on next page)

Figure S1. Specificity of activation of observer VMHvl^{PR} neurons by aggressive displays, related to Figure 1

(A) The majority of GCaMP6s+ VMHvl neurons expresses Esr1 and therefore corresponds to VMHvl^{PR} neurons.

(B) No difference in number of GCaMP6s+ VMHvl neurons between males used as aggressors and observers.

(C–F) Fluorescence intensity changes in VMHvl^{PR} neurons do not reflect motion artifacts. Schematic of strategy to express GFP in VMHvl^{PR} neurons (C). No discernible change in GFP fluorescence during attacks (D) or tail-rattles (E). GFP expression in VMHvl^{PR} neurons (F).

(G–H) Representative activity trace of VMHvl^{PR} neurons from an aggressor (G) or observer (H) witnessing demonstrators fight.

(I–M) BNST^{Tac1} neurons do not exhibit aggression-mirroring. Strategy to express GCaMP6s in BNST^{Tac1} neurons (I). Activation of aggressor BNST^{Tac1} neurons upon entry of the intruder in the home cage (J) and during attacks but not tail-rattles (K). No discernible activation of observer BNST^{Tac1} neurons during attacks or tail-rattles (L). GCaMP6s expression in BSNT^{Tac1} neurons (M).

(N–P) No discernible activation of VMHvl^{PR} neurons in mice who are using (N) or observing another mouse use (O) a running wheel despite expression of GCaMP6s+ in these cells (P).

(Q–R) No discernible activation of VMHvl^{PR} neurons in mice who are observing Trpc2 null demonstrators. Mean ± SEM n = 5 (A, C–F), 14 (B), 7 (N–P), 6 (Q and R) *PR^{Cre}* males, and 4 (I–M) *Tac1^{Cre}* males. *p < 0.05, ***p < 0.001, ****p < 0.0001. Scale bar, 100 μm.

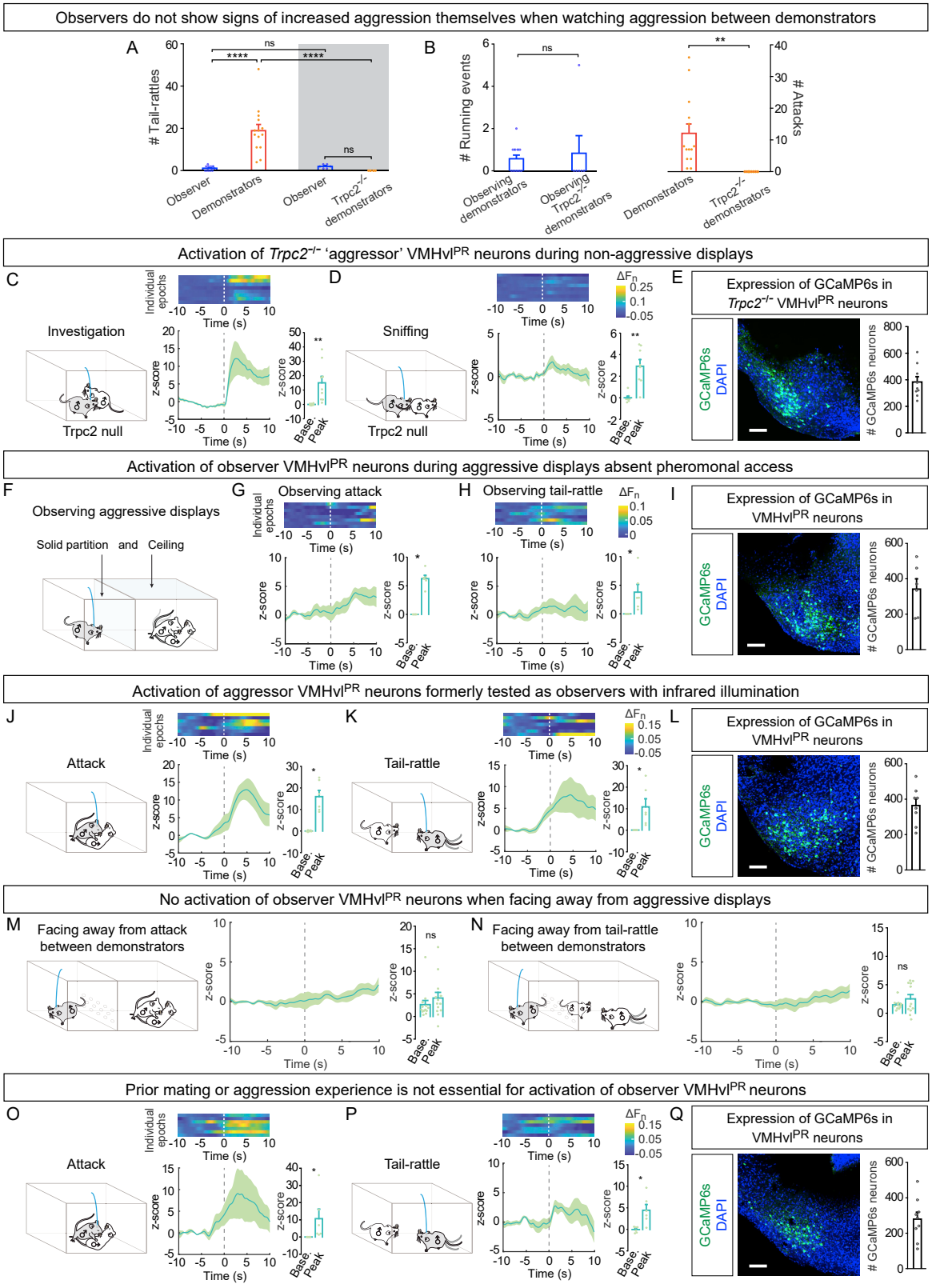

(legend on next page)

Figure S2. Sensory and experiential modulation of activity of observer VMHvl^{PR} neurons, related to Figure 2

(A and B) Observers show minimal and comparable tail-rattling when watching aggression between demonstrators or non-aggressive interactions between *Trpc2*$^{-/-}$ demonstrators (A). Despite the large number of attacks between aggressive demonstrators WT for Trpc2, observers show few to no sudden, rapid movements that could be construed as chasing during an aggressive bout (denoted by "# running events"). Observers showed comparably few to no sudden, rapid movements even when watching non-aggressive interactions between *Trpc2*$^{-/-}$ demonstrators (B).

(C–E) Trpc2 null males do not fight but their VMHvl^{PR} neurons are still activated during investigation (C) and sniffing (D) of the intruder male. GCaMP6s expression in VMHvl^{PR} cells (E).

(F–I) Observer VMHvl^{PR} neurons are activated during aggression even when separated from demonstrators by solid partitions. Schematic of behavioral paradigm (F). Observer cells are activated during attacks (G) and tail-rattles (H). GCaMP6s expression in VMHvl^{PR} cells (I).

(J–L) Although observer VMHvl^{PR} neurons are not activated when witnessing aggression under infrared illumination (Figures 2D–2F), the same population of cells is activated subsequently as aggressor VMHvl^{PR} cells when attacking (J) and tail-rattling (K) to a WT male intruder. GCaMP6s expression in VMHvl^{PR} neurons of these mice (L).

(M and N) No discernible activation of observer VMHvl^{PR} neurons during attacks (M) or tail-rattles (N) by aggressive demonstrators when the experimental male is facing away from the demonstrators. These findings are from analyses performed on observer VMHvl^{PR} neurons from the same mice shown in Figures 1E, 1F, and 1L–1N.

(O–Q) Observer VMHvl^{PR} neurons of socially naive male mice are activated subsequently as aggressor neurons when attacking (O) or tail-rattling (P) to a WT male intruder. GCaMP6s expression in VMHvl^{PR} neurons of these mice (Q). Mean ± SEM n = 9 *Trpc2*$^{-/-}$;*PR*^{Cre} (C–E), 13 *PR*^{Cre} (A and B, assays with Trpc2 WT demonstrators), 6 *PR*^{Cre} (A and B, assays with Trpc2 null demonstrators), 6 *PR*^{Cre} (F–I), 8 *PR*^{Cre} (J–L), 13 *PR*^{Cre} (M–N), and 8 *PR*^{Cre} (O–Q) males. Scale bars, 100 μm.

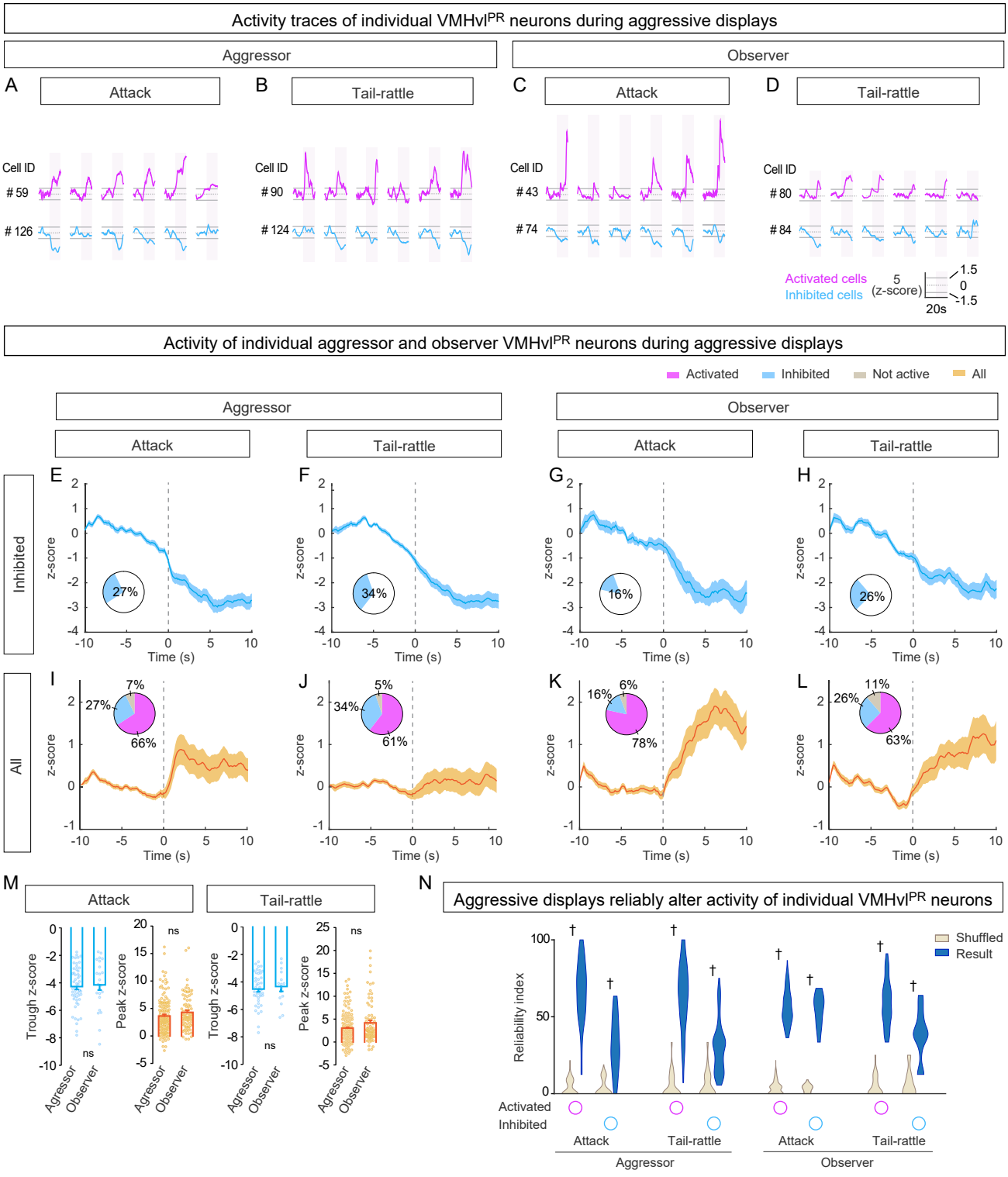

Figure S3. Activity of individual aggressor and observer VMHvl^{PR} neurons, related to Figure 3

(A–D) Fluorescence change of individual aggressor or observer VMHvl^{PR} neurons during multiple, consecutive epochs of attacks (A, C) and tail-rattles (B,D). (E–M) Mean fluorescence changes in inhibited (E–H) or all segmented VMHvl^{PR} (I–L) neurons during attacks or tail-rattles in aggressor and observer paradigms. Inset pie-charts show percent of inhibited (blue), activated (pink), or silent (gray) VMHvl^{PR} neurons during these behaviors. For inhibited neurons (blue), no

(legend continued on next page)

difference in peak reduction in fluorescence between aggressors and observers for either attacks or tail-rattles (M). Mean fluorescence of all segmented VMHvl^{PR} neurons (yellow/red) shows that this population is activated in aggressors (I,J) and observers (K,L) during attacks and tail-rattles in a comparable manner (M). (N) Activation or inhibition of individual aggressor and observer VMHvl^{PR} neurons during an aggressive epoch (of attack or tail-rattle) are significantly more likely to be repeated, respectively, during successive epochs of that display compared to activity patterns obtained by chance, as determined by shuffling fluorescence signals across the behavioral assay. Mean ± SEM n = 5 *PR*^{Cre} males. †p < 0.0001.

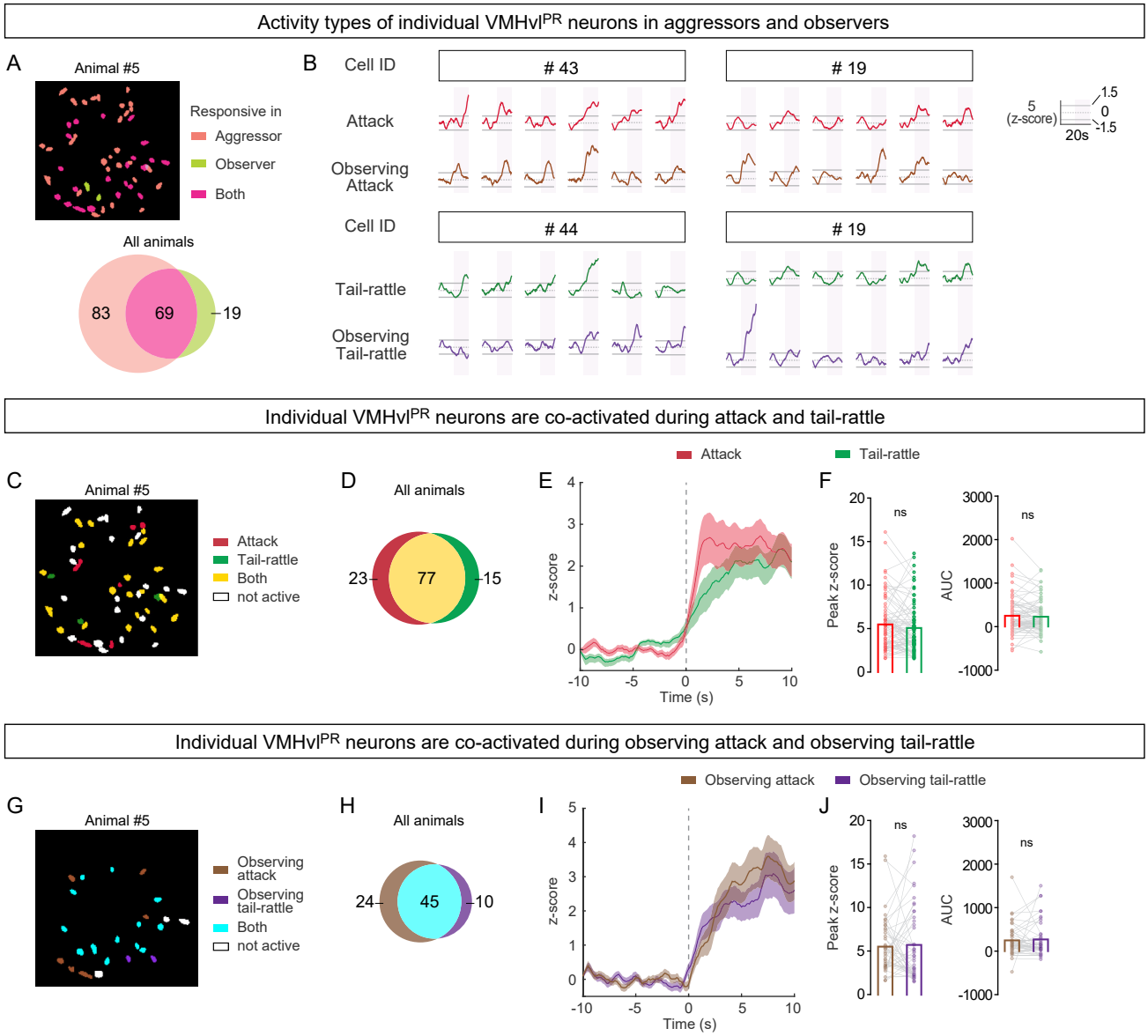

Figure S4. Co-activation of individual VMHvl^{PR} neurons during aggressive displays, related to Figure 4 and Table S1

(A) Distribution of VMHvl^{PR} neurons between aggressor and observer paradigms, with 69 cells imaged in both assays. Inset shows segmented VMHvl^{PR} cells in representative imaging plane.

(B) Activity traces of individual VMHvl^{PR} neurons co-activated in aggressor as well as observer paradigms during attacks (cell 43) or tail-rattles (cell 44) or both (cell 19).

(C–F) Co-activation of individual aggressor neurons during attacks and tail-rattles. Segmented cells during representative imaging sessions of an aggressor (C). Overlapping sets of aggressor VMHvl^{PR} neurons are co-activated during attacks and tail-rattles (D), with comparable activation dynamics (E) and peak amplitude of, or net, activation (F).

(G–J) Co-activation of individual observer neurons during attacks and tail-rattles. Segmented cells during representative imaging sessions of an observer (G). Overlapping sets of observer VMHvl^{PR} neurons are co-activated during attacks and tail-rattles (H), with comparable activation dynamics (I) and peak amplitude of, or net, activation (J). n = 5 PR^{Cre} males (A–F).

Observer VMHvl neurons are specifically co-activated during aggression

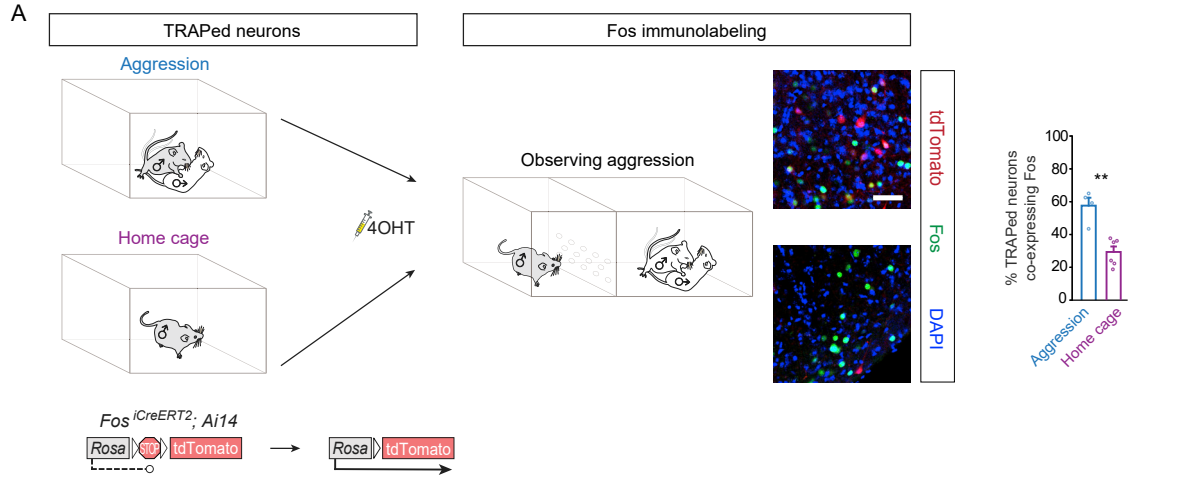

Aggression mirror-TRAPed VMHvl neurons are active during aggressive interactions with intruder males

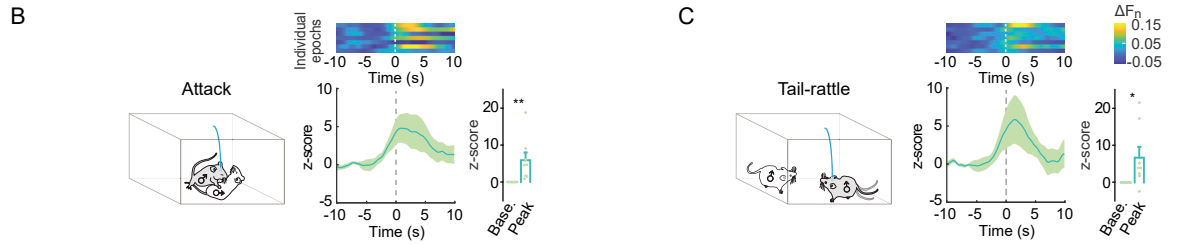

Aggression mirror-TRAPed VMHvl neurons are not active during non-aggressive interactions between demonstrators

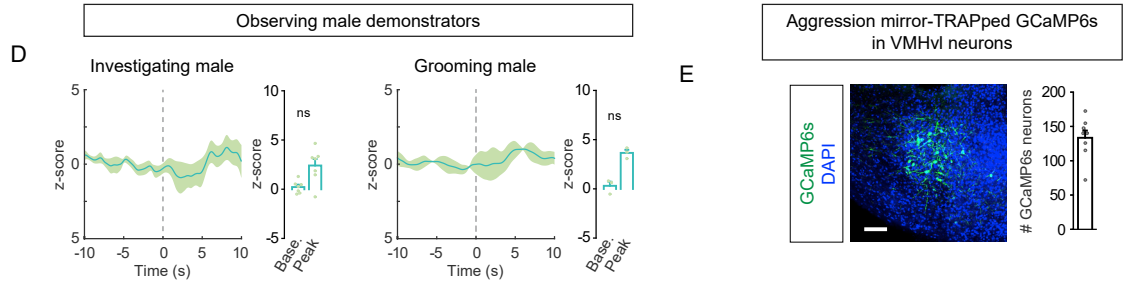

A majority of VMHvl observer neurons is VMHvl^{PR} neurons

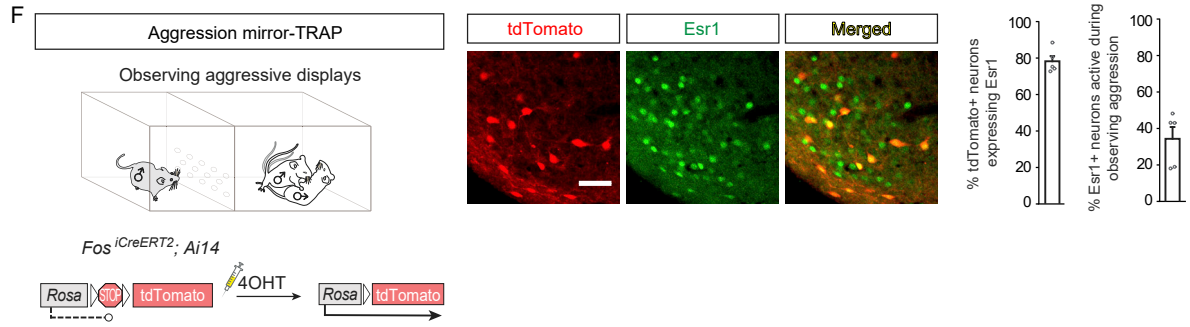

(legend on next page)

Figure S5. Characterizing VMHvl neurons tagged with aggression mirror-TRAP, related to Figure 5

(A) Greater overlap of Fos labeled observer VMHvl neurons with aggression-activated, FosTRAP2-tagged neurons (Aggression-TRAP) compared to home cage-activated FosTRAP2 tagged cells. Note that aggression-TRAPed mice are identical to those in Figures 5B and 5C.

(B and C) Aggression mirror-TRAPed VMHvl neurons are not only activated when observing aggression (Figures 5E and 5F) but also during intruder-directed displays of attack (B) or tail-rattle (C) by self. Same experimental males as used in Figures 5E and 5F.

(D and E) Aggression mirror-TRAPed VMHvl neurons in observers show no discernible activation during investigation or grooming between demonstrators (D). GCaMP6s expression in aggression mirror-TRAPed VMHvl neurons (E).

(F) Aggression mirror-TRAPed VMHvl neurons are largely a subset of $VMHvl^{PR}$ neurons (which also co-express Esr1). Mean ± SEM n = 4 (A, aggression-TRAP), 6 (A, home cage TRAP) $Fos^{iCreERT2}$;*Ai14* males; 8 (B–E) $Fos^{iCreERT2}$ males; 5 (F) $Fos^{iCreERT2}$;*Ai14* males. *p < 0.05, **p < 0.01. Scale bars, 50 μm (A,F) and 100 μm (E).

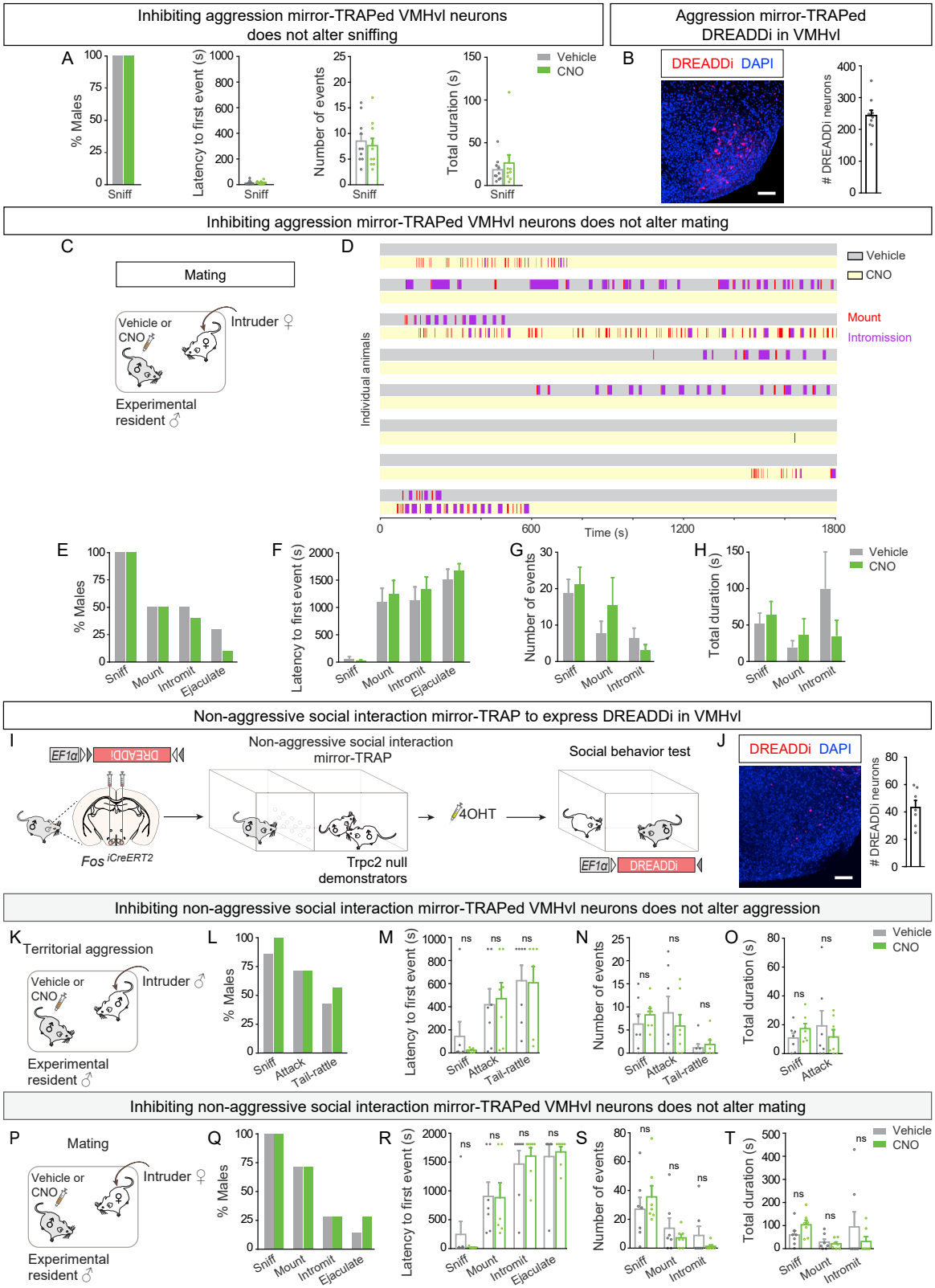

(legend on next page)

Figure S6. Activity of aggression mirror-TRAPed VMHvl neurons is not essential for mating, related to Figure 6

(A and B) Inhibition of aggression mirror-TRAPed VMHvl neurons does not alter sniffing of male intruder (A). Expression of DREADDi in aggression mirror-TRAPed VMHvl cells (B).

(C) Schematic of mating assay with the aggression mirror-TRAPed resident male expressing DREADDi in VMHvl cells.

(D) Rasters of individual resident males showing no alteration of sexual displays (mount, intromission) upon inhibition of aggression-mirroring VMHvl neurons.

(E–H) Inhibition of aggression-mirroring VMHvl neurons does not alter likelihood (E), latency (F), number (G), or duration (H) of male-initiated interactions during mating.

(I and J) Schematic of strategy to express DREADDi in VMHvl neurons of observers watching interactions between Trpc2 null demonstrators (I) and quantitation of DREADDi expression in VMHvl cells (J).

(K–O) Provision of vehicle (saline) or CNO to experimental resident males followed by introduction of WT intruder males (K) does not alter probability of initiating aggression (L) or other behavioral parameters of fighting such as latency (M), number of events (N), or duration (O).

(P–T) Provision of vehicle (saline) or CNO to experimental resident males followed by introduction of WT receptive females (P) does not alter probability of initiating mating (Q) or other behavioral parameters of mating such as latency (R), number of events (S), or duration (T). Mean ± SEM $Fos^{iCreERT2}$ males, 10 (A–H, identical to males of Figure 6) and 7 (J–T). Scale bar, 100 μm.

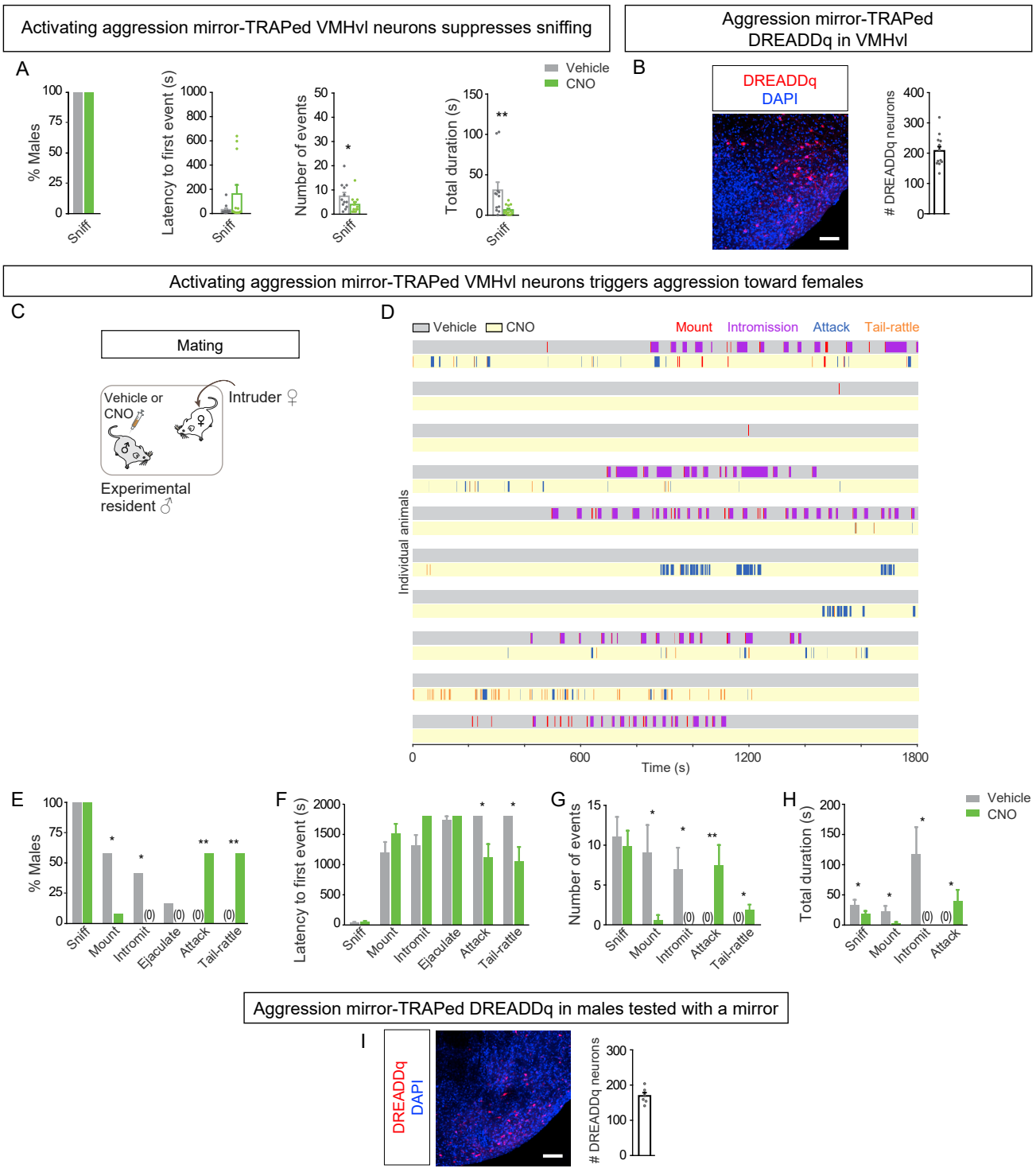

Figure S7. Activation of aggression mirror-TRAPed VMHvl neurons triggers aggression toward females, related to Figure 7

(A and B) Activation of aggression mirror-TRAPed VMHvl neurons reduces number and duration of sniffing of the male intruder (A). Expression of DREADDq in aggression mirror-TRAPed VMHvl cells (B).

(C) Schematic of mating assay with the aggression mirror-TRAPed resident male expressing DREADDq in VMHvl cells.

(D) Rasters of individual resident males show that activation of VMHvl neurons with CNO elicits aggressive displays toward females.

(legend continued on next page)

(E–H) Activation of aggression mirror-TRAPed VMHvl neurons reduces the likelihood of mating and increases that of aggression toward WT female intruders (E). There was also a decreased latency to fight (F), fewer mounts and intromissions and greater attacks and tail-rattles (G), reduced duration of sniffing, mounting, and intromission (H), and longer duration of attacks (H).

(I) Expression of DREADDq in aggression mirror-TRAPed VMHvl neurons in males tested with a mirror in their home cage (Figures 7H and 7I). Mean ± SEM n = 12 $Fos^{iCreERT2}$ males, identical to those of Figure 7 (A–I), and 6 $Fos^{iCreERT2}$ males. *p < 0.05, **p < 0.01. Scale bars, 100 μm.